Quaternary Science Advances 1 (2020) 100002

Contents lists available at ScienceDirect

Quaternary Science Advances

journal homepage: www.journals.elsevier.com/quaternary-science-advances

Geologic controls on ice sheet sensitivity to deglacial climate forcing in the Ross Embayment, Antarctica

Daniel P. Lowry [a,*,1], Nicholas R. Golledge [a,b], Nancy A.N. Bertler [a,b], R. Selwyn Jones [c], Robert McKay [a], Jamey Stutz [a]

[a] Antarctic Research Centre, Victoria University of Wellington, Wellington, 6140, New Zealand
[b] GNS Science, Lower Hutt, 5040, New Zealand
[c] Department of Geography, Durham University, Durham, DH1, United Kingdom

ARTICLE INFO

Keywords:
Quaternary
Deglaciation
Antarctica
Ice sheet modeling
Geomorphology
Glacial
Paleoclimate

ABSTRACT

The role of external forcings in the deglacial ice sheet evolution of the Ross Embayment, Antarctica's largest catchment, continues to be a highly contested topic. Although numerical ice sheet models indicate that ocean and atmosphere forcings were the main drivers of deglacial ice sheet retreat, these models have difficulty in accurately capturing both the timing and rate of retreat in every area of the embayment. Other factors that influence the sensitivity of ice sheets to climate forcing, such as the physical properties of the bed, isostatic deformation of the continental shelf, and rheological properties of the ice, are parameterized inconsistently across models. Here, we explore using a systematic approach the extent to which specific model parameters related to basal substrate, bed deformation and ice flow and rheology impact the climate sensitivity of the ice sheet in the Ross Embayment over the last deglaciation. Higher variability in deglacial ice sheet evolution is observed among experiments using different model parameters than among experiments using different climate forcings. Mantle viscosity, the material properties of the till, and an enhancement factor of the shallow shelf approximation (E_{SSA}) component of the stress balance exhibit strong influences on the timing of ice sheet response to deglacial climate forcing, and may contribute to the asynchronous retreat behavior of the Eastern and Western Ross Sea. The Western Ross Sea is especially sensitive to both climate forcing and model parameter selection, with both cool climate forcing and low E_{SSA} producing better agreement with terrestrial ice thinning records. The evolution and extent of the Siple Coast grounding line is highly sensitive to the mantle viscosity and till properties in addition to ocean and precipitation forcing. Constraining these physical model parameters is therefore paramount for accurate projections of the Antarctic ice sheet response to projected future changes in ocean temperatures and precipitation.

1. Introduction

Fed by ice streams and outlet glaciers from both the West and East Antarctic Ice Sheets (WAIS and EAIS, respectively), the Ross Embayment is the largest drainage basin in Antarctica (Anderson et al., 2019). Estimates of the outflow of ice from the Siple Coast and the Transantarctic Mountains into the modern Ross Ice Shelf are 80 ± 2 and 49 ± 4 Gt yr^{-1}, respectively (Rignot et al., 2008). However, the response of these outflows from WAIS and EAIS to future climate warming scenarios in numerical ice sheet models remains uncertain, with large differences in ice sheet sensitivity to climate forcing related to model parameterizations (Golledge et al., 2015, 2019; DeConto and Pollard, 2016; Edwards et al., 2019; Seroussi et al., 2019). Constraining past grounding-line retreat in the Ross Embayment can help inform future predictions. In the Ross Embayment, the grounding line has retreated by more than 1000 km since the Last Glacial Maximum (LGM; Bentley et al., 2010), however, the influences of external and internal forcings of the ice sheet on both the timing and pattern of this retreat are still unclear (Conway et al., 1999; McKay et al., 2016; Kingslake et al., 2018; Goehring et al., 2019; Lowry et al., 2019a).

Previous studies have argued for a number of controls on the ice sheet retreat behaviour in the Ross Embayment. The traditional "swinging gate" model, first proposed by Conway et al. (1999) and primarily based on Transantarctic ice thinning records, suggested that Ross Sea

* Corresponding author.
E-mail address: d.lowry@gns.cri.nz (D.P. Lowry).
[1] Current affiliation: GNS Science, Lower Hutt, 5040, New Zealand.

https://doi.org/10.1016/j.qsa.2020.100002
Received 6 November 2019; Received in revised form 6 January 2020; Accepted 9 January 2020
Available online 8 February 2020
2666-0334/© 2020 The Author(s). Published by Elsevier Ltd. This is an open access article under the CC BY-NC-ND license (http://creativecommons.org/licenses/by-nc-nd/4.0/).

grounding-line retreat was constrained to the late Holocene, in the absence of climate or sea level forcing. Interpretations have since evolved with radiocarbon dating of marine sediments and geomorphology data from the Ross Sea, and the current understanding is that a combination of marine forcing and physiographic controls resulted in an earlier retreat with a landward grounding-line migration from the central embayment (McKay et al., 2016; Halberstadt et al., 2016; Lee et al., 2017; Bart et al., 2018). However, the relative influences of specific external forcings are still unclear, with both sea level forcing (Goehring et al., 2019) and a combination of oceanic and atmospheric warming both proposed as the primary control of grounding-line migration in the Ross Embayment (Yokoyama et al., 2016; Lowry et al., 2019a). In particular, incursions of relatively warm Circumpolar Deep Water (CDW) are also thought to have contributed to ice sheet retreat in the Amundsen Sea Sector during the last deglaciation (Hillenbrand et al., 2017), and may have also been a factor in the Ross Sea (Tinto et al., 2019).

Contributing to this ongoing debate, differences in the retreat behaviour between the eastern and western Ross Sea (ERS and WRS, respectively) have been identified, suggesting an earlier retreat in the ERS relative to the WRS (Domack et al., 1999; Halberstadt et al., 2016; Bart et al., 2018). This has generally been attributed to differences in seafloor bathymetry and geology. The western Ross Sea (WRS) has a greater abundance of ice rises that can stabilise the ice sheet (Halberstadt et al., 2016; Simkins et al., 2016; Greenwood et al., 2018; Anderson et al., 2019). Changes in ocean circulation related to the influx of meltwater into the Southern Ocean may have led to differences in sub-surface ocean temperatures that enhanced grounding-line retreat in the eastern basin relative to the western basin (Golledge et al., 2014), in addition to potential localised incursions of relatively warm modified CDW related to changes in continental shelf geometry relative to offshore currents (Tinto et al., 2019). The isostatic response of the solid Earth to changes in deglacial Antarctic ice loss has also been suggested to have driven extensive deglacial retreat of WAIS, and may explain the widespread presence of young organic carbon in the upper till beneath West Antarctic ice streams (Kingslake et al., 2018). Although the extent to which these mechanisms enhanced or diminished grounding-line retreat in different regions of the embayment is poorly constrained, they likely contribute to the data-model discrepancies observed in regional ice sheet model experiments (Lowry et al., 2019a).

Ice sheet models have been demonstrated to be highly sensitive to the physical representation of the bed as well as the evolution and deformation of the continental shelf, which can influence ice sheet sensitivity to climate forcing (Matsuoka et al., 2015; Bart et al., 2016; Kingslake et al., 2018; Colleoni et al., 2018). In the Ross Sea specifically, a tectonic boundary runs north-south through the central embayment, leading to differences in crustal properties in the ERS and WRS (Behrendt and Cooper, 1991; Tinto et al., 2019). This implies that past ice flows of WAIS and EAIS were modulated by different subglacial conditions. In addition, observations suggest that the faster flowing ice streams that flow into the Ross Embayment are especially sensitive to the conditions of the underlying till (Alley et al., 1986; Hulbe et al., 2016). In this paper, we explore how the Antarctic ice sheet response to deglacial climate forcing could be influenced by basal substrate and hydrological properties, the solid Earth response to changes in ice loading, and by the way that ice flow and rheology are parameterised. Understanding the effect of each model parameter on ice sheet sensitivity to climate forcing is highly valuable, as it addresses the data-model mismatches, and it can help prioritize the constraints required for accurate projections of the future Antarctic response to anthropogenic climate warming.

2. Methods

2.1. Regional ice sheet modeling

To determine the controls on ice sheet sensitivity to deglacial climate forcing in the Ross Embayment, we analyse two ensembles of regional ice sheet simulations. The simulations of both ensembles were performed at 10 km resolution using the Parallel Ice Sheet Model (PISM), a sophisticated ice sheet model which allows for realistic ice streams that exhibit the full range of observed ice stream velocities (Bueler and Brown, 2009; Winkelmann et al., 2011). Prior to the deglacial experiments, we perform a full-continent spin-up run following the protocol of Martin et al. (2011). We then construct a regional drainage basin model of the Ross Embayment based on the ice sheet thickness and topography. The regional domain in these simulations encompasses the Ross Ice Shelf and the surrounding ice drainage basins of grounded ice, which are allowed to dynamically evolve. A larger area around the drainage basins is maintained at a constant thickness as a time-independent boundary condition of the model. This regional modeling approach allows for higher computational efficiency due to the smaller domain size, while simultaneously allowing for the grounding-line position to change through time.

The first model ensemble of regional ice sheet simulations considers a wide range of deglacial ocean/atmosphere forcings (referred hereafter as the climate forcing ensemble), and is previously described in Lowry et al. (2019a). These simulations are initialized following a pre-glacial ice sheet simulation from the last interglacial (131 ka) to 35 ka. From this 35 ka configuration, different ocean/atmosphere forcing combinations are applied for the deglacial experiments (35–0 ka). These forcings are derived from the temperature reconstructions of the EPICA Dome C (EDC) ice core from East Antarctica (75°S, 123°E; Parrenin et al., 2007) and the WAIS Divide (WDC) ice core from West Antarctica (~79°S, 112°W; Cuffey et al., 2016), global and Southern Ocean benthic ocean temperature proxy reconstructions (GOT and SOT, respectively; Liesecki and Raymo, 2005; Elderfield et al., 2012), and model output of two deglacial climate model simulations, namely, Trace-21ka and LOVECLIM DGns (Liu et al., 2009; Menviel et al., 2011).

The ocean forcing is in the form of basal ice shelf melt rate anomalies and is applied uniformly. The atmosphere forcings include surface temperature and precipitation anomalies and a back pressure forcing to heuristically represent the ice-flow regulating effects of sea ice. Conversion from temperature anomalies to basal ice shelf melt rates and back pressure forcing is determined using a scaling relationship derived from a series of sensitivity experiments (see Lowry et al., 2019a). Precipitation forcing is also determined via a scaling relationship to temperature for the majority of simulations (i.e., 7%/°C), however, in three simulations we apply precipitation forcing derived from the WDC accumulation record (Fudge et al., 2016). In total, the climate forcing ensemble consists of 39 simulations, each with a different ocean/atmosphere forcing combination.

In addition to the climate forcing model ensemble, we perform simulations that use the same climate forcing (average of the individual ocean/atmosphere forcings), but with a single model parameter adjusted within a reasonable range for the Ross Embayment to assess the influence of each parameter on deglacial ice sheet retreat (hereafter referred to as the model parameter ensemble). These runs are initialized from 131 ka and run to 0 ka. We consider five parameters related to ice rheology and subglacial conditions to investigate their influence on the ice sheet response to deglacial climate forcing. To compare with the simulation using average ocean and atmosphere forcings from the climate model ensemble, we perform three simulations with different enhancement factors of the shallow ice approximation (SIA) and shallow shelf approximation (SSA) components of the stress balance, respectively, three simulations with higher sliding exponent parameters (q), three simulations with lower minimum till friction angles ($\varnothing_{min}$), three simulations with different mantle viscosity values, one simulation with no bed deformation, and one simulation with reduced bed smoothing. In total, this model parameter ensemble is comprised of 18 simulations. Each model parameter is explained in greater detail in the subsequent subsection.

2.2. Model parameters

2.2.1. Stress balance terms

All of the ice sheet model simulations in both ensembles employ a hybrid approximation of the Stokes stress balance, which was developed to model the large range of ice flow velocities observed in ice sheets (Bueler and Brown, 2009). In this hybrid stress balance scheme, velocities are calculated by the superposition of the SIA, which dominates in grounded regions, and the SSA, which dominates in ice shelves and ice streams and serves as a basal sliding velocity of grounded regions (Winkelmann et al., 2011). By using the SSA as a sliding law for grounded regions, this scheme avoids discontinuities at the onset of sliding, and is thus advantageous for modeling marine ice sheets with transitions between grounded and floating ice. To account for anisotropy and other uncertainties related to variations in viscosity and basal resistance, enhancement factors of the SIA and SSA can be applied (E_{SIA} and E_{SSA}, respectively); in general, E_{SIA} is greater than 1, and E_{SSA} is less than 1 (Martin et al., 2011). Larger E_{SSA} values produce faster ice streams and thinner ice shelves, and smaller E_{SIA} values produce thicker grounded ice (Kingslake et al., 2018). In the climate forcing ensemble, we use standard values of $E_{SIA} = 4.0$ and $E_{SSA} = 0.8$ for the experiments. In the model parameter ensemble, we perform six additional experiments with E_{SIA} values of 2.0, 3.0, and 5.0, and E_{ssa} values of 0.4, 0.6, and 1.0.

2.2.2. Basal substrate terms

The sliding parameterization in PISM is in the form of a power law that ranges from plastic Coloumb sliding to a linear sliding law (PISM authors, 2017; Kingslake et al., 2018):

$$\tau_b = -\tau_c \frac{u}{u_{threshold}^{q} |u|^{q-1}}$$

In the above power law, τ_b is the basal shear stress, τ_c is the yield stress, u is velocity, where $u_{threshold}$ is a threshold velocity, and q is the sliding exponent parameter, where $q = 0$ is purely plastic sliding, and $q = 1$ is sliding linearly related to the applied stress. The default value for this parameter is $q = 0.25$, which is the value used in the climate forcing model ensemble. In the model parameter ensemble, we also consider higher values of $q = 0.5$, $q = 0.75$ and $q = 1.0$, as in Kingslake et al. (2018).

Another important sliding-related parameter is the till friction angle, which is related to the material properties of the till and influences τ_c:

$$\tau_c = c_0 + (tan\Phi)N_{till}$$

where c_0 is the till cohesion (set to 0 in PISM by default), N_{till} is the effective pressure of the till, and Φ is the till friction angle parameter (PISM authors). In PISM, τ_c can be spatially variable rather than uniform by adjusting Φ (Kingslake et al., 2018). Previous ice sheet modeling work has heuristically determined Φ as a piecewise linear function of the bed elevation (Winkelmann et al., 2011; Martin et al., 2011; Aschwanden et al., 2013; Kingslake et al., 2018), which is a method we apply here:

$$\Phi(x,y) = \begin{cases} \Phi_{min}, & b(x,y) \le b_{min}, \\ \Phi_{min} + (b(x,y) - b_{min})M, & b_{min} < b(x,y) < b_{max}, \\ \Phi_{max}, & b_{max} \le b(x,y). \end{cases}$$

where b is the bed elevation, M is defined as $(\Phi_{max} - \Phi_{min})/(b_{max} - b_{min})$, and (x,y) refers to a given point in space (PISM authors, 2017). While the default Φ value in PISM is 30°, the minimum till friction angle (Φ_{min}) is set to 9° for topography less than 200 m below sea level and the maximum till friction angle (Φ_{max}) is set to 30° for topography at sea level for the climate forcing ensemble. This is based on the assumption that lower-lying till with a marine history is weaker (Huybrechts and de Wolde, 1999; PISM authors, 2017). In the model parameter ensemble, we experiment with lower values of Φ_{min}, i.e., 3°, 4°, and 6° at 200 m below sea level. This is more in line with the range for Φ_{min} used in Kingslake et al. (2018), i.e., 1–3°, though we note that Φ estimated from laboratory tests of till recovered from below West Antarctic ice streams is 24° (Tulaczyk et al., 2000).

2.2.3. Solid earth

The isostatic response of the solid Earth to the growth and decay of the Antarctic ice sheet has been argued to be the fundamental control of the grounding-line dynamics of WAIS (Gomez et al., 2010; McKay et al., 2016; Kingslake et al., 2018; Whitehouse et al., 2019). The Earth deformation scheme employed by PISM is based on the viscoelastic deformable Earth model of Bueler et al. (2007), which improves on the traditional elastic plate lithosphere with relaxing asthenosphere (ELRA) scheme used in many ice sheet models (e.g., de Boer et al., 2015; DeConto and Pollard, 2016). The scheme in PISM uses a two-layer approach that approximates the upper mantle as a linearly viscous half-space overlain by an elastic plate lithosphere. In our experiments, we focus on the mantle viscosity term and its relation to ice sheet loading, Earth deformation and bed topography.

In Lowry et al. (2019a), the application of a higher mantle viscosity (5e20 Pa s) led to a rapid response to deglacial climate forcing, with a retreat beyond the modern grounding-line position of Siple Coast, and readvancement of WAIS through the Holocene, consistent with the findings of Kingslake et al. (2018). In contrast, the climate forcing ensemble, in which a standard mantle viscosity value of 1e19 Pa s is applied, exhibited no such WAIS readvance behavior (Lowry et al., 2019a). At 100 km depth, the mantle viscosity of the Ross Embayment is spatially variable, with values ranging from 1e18 to 1e22 Pa s (Whitehouse et al., 2019). In general, the highest mantle viscosity values are observed over EAIS, with the lowest observed over the western Ross Sea and parts of WAIS. To better capture the full mantle viscosity range of the Ross Embayment, we consider three additional mantle viscosity values of 1e18, 1e20, and 1e21 Pa s.

3. Results

3.1. Effect of external forcing on ice sheet retreat

In the climate forcing ensemble, the ice sheet model simulations are consistent in terms of the LGM grounding-line position, which extends to nearly the continental shelf edge in the eastern, central, and western parts of the embayment (Fig. 1). However, it is important to note that although LGM reconstructions of the Ross Sea sector suggest that this is the case for the eastern and central parts of the Embayment (Licht et al., 2002; Bart et al., 2018), evidence from the outer WRS does not agree on where the grounding line was located at this time (Shipp et al., 1999; Anderson et al., 2014; Goehring et al., 2019).

In terms of the deglaciation, the combination of atmosphere and ocean forcing controls both the timing and spatial pattern of grounding-line retreat in the regional ice sheet model simulations. The atmosphere forcings, in the form of surface temperature and back pressure anomalies, exert a strong influence on the timing of the initial ice sheet retreat from the continental shelf edge. In particular, the simulation forced with the highest surface temperature and lowest back pressure in the early deglacial period (i.e. the warm scenario) displays earlier retreat that is relatively synchronous across the outer embayment (Fig. 1a). The simulation forced with relatively cooler early deglacial surface temperature anomalies, high back pressure and cooler ocean forcing (i.e. the cool scenario) shows delayed retreat in the WRS and ERS as compared to the central embayment (Fig. 1b), resembling the empirically-based reconstructions of McKay et al. (2016), Halberstadt et al. (2016) and Lee et al. (2017). In this cool scenario, grounding line retreat is most rapid in the early Holocene (~12–10 ka).

Although ice sheet retreat cannot initiate in the absence of climate forcing (see Lowry et al., 2019a), sea level forcing is an important contributor to the modelled ice sheet retreat in the Ross Embayment. Fig. 1c and d shows two simulations, each forced by moderate

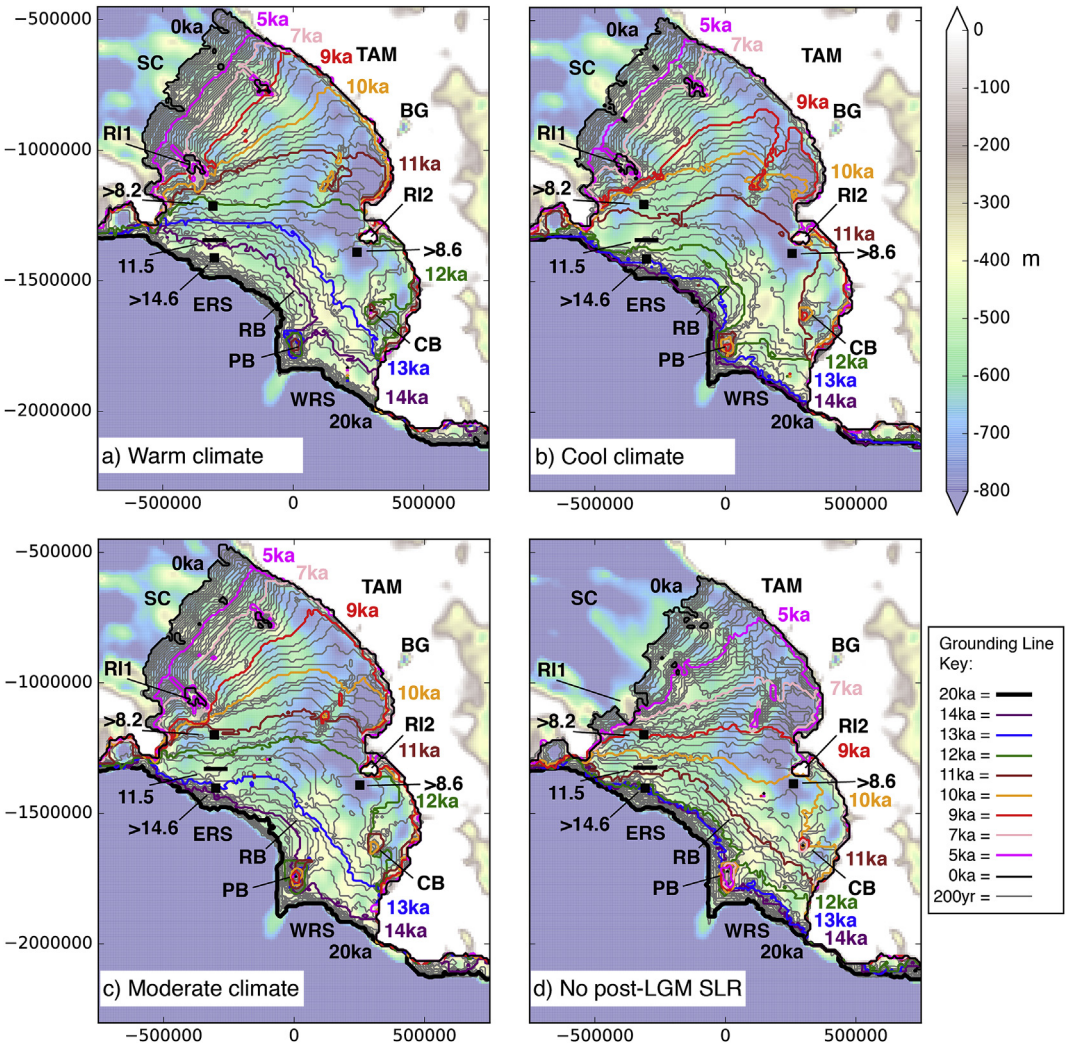

Fig. 1. Grounding line evolution with (a) warm (LOVECLIM ocean/atmosphere forcing), (b) cool (TraCE-21ka ocean/atmosphere forcing), and (c) moderate (model-proxy average ocean/atmosphere forcing) climate forcing, respectively. Gray lines indicate grounding line position every 200 years from 20 ka to 0 ka, while coloured lines show the grounding line position at given time slices (see grounding line key). (d) Grounding line evolution with moderate climate forcing, but constant LGM sea level forcing, i.e., no post-LGM sea level rise (SLR). The grounding line positions are overlain on the basal topography at the end of the simulation (0 ka). Black squares indicate radiocarbon ages for minimum age constraints of grounding-line retreat from McKay et al. (2016) and Bart et al. (2018). Ages derived from acid-insoluble organic (AIO) residues from bulk carbon are not included given their high uncertainty and potential for bias. The horizontal black line indicates the early Holocene grounding-line position suggested in Bart et al. (2018). Dates are given in ka. Locations for the Eastern Ross Sea (ERS), Western Ross Sea (WRS), Roosevelt Island (RI1), Siple Coast (SC), the Transantarctic Mountains (TAM), Ross Island (RI2), Ross Bank (RB), Pennell Bank (PB), and Crary Bank (CB) are indicated.

ocean/atmosphere forcing; the difference is that the first simulation uses a time-dependent sea level forcing with rising sea level from LGM to 0ka (Fig. 1c), whereas in the second simulation, the sea level forcing is maintained at the LGM level of −125 m (Fig. 1d). The initial retreat between 18 and 14 ka is similar between the simulations with and without sea level forcing, despite the rapid global sea level rise event of Meltwater Pulse 1a during this interval (~14.6 ka; Deschamps et al., 2012). However, the grounding-line retreat subsequently becomes delayed for the remainder of the simulation in the absence of a rising sea level. The delay increases through time, with a delay of ~2ka in the outer embayment, but ~3–5 ka in the inner embayment (Fig. 1c vs. 1d). The position at 0 ka is advanced along the Siple Coast relative to modern observations as well as the simulations with both climate and sea level forcing (Fig. 1d vs. Fig. 1a–c). As a result, WAIS remains thicker through the Holocene, resulting in higher ice loading and isostatic subsidence, and thus lower basal topography in this region.

With development of the ice shelf and ocean cavity, the sub-shelf melt rate forcing is the dominant control on grounding-line position. Sea level forcing also enhances the effect of ocean thermal forcing. With a constant LGM sea level, as the grounding line retreats to the Siple Coast, Roosevelt Island acts as a pinning point over the last 7 ka of the simulation (Fig. 1d), hence ocean forcing alone is insufficient for achieving an accurate grounding line position along the northern Siple Coast. With the addition of sea level forcing, the pinning effect only lasts for approximately 4.2 ka before the grounding line retreats beyond Roosevelt Island. By the end of the simulation with combined ocean and sea level forcing, the grounding-line position is consistent with observations in this region (Fig. 1c).

3.2. *Effect of model parameter selection on ice sheet retreat*

Selection of model parameters and parameterizations of physical processes in ice sheet models has previously been shown to govern the ice sheet sensitivity to climate forcing (e.g. Rignot et al., 2008; DeConto and Pollard, 2016; Kingslake et al., 2018). Here, we demonstrate the effect of individual parameters on deglacial ice sheet retreat in the Ross Embayment from a spatiotemporal perspective. A summary of the experiments and results are shown in Table 1.

The two stress balance terms, E_{SIA} and E_{SSA}, have different effects on

Table 1
Model parameter ensemble experiments and summary of results. The asterisks indicate the parameter values used in the climate forcing ensemble as well as the standard values of the non-experimental parameters in the model parameter ensemble. PD refers to present day (0 ka) and SC refers to the Siple Coast.

Parameter	Experiment values	Effect of increasing value on LGM state	Effect of increasing value on deglaciation	Effect of increasing value on PD state	Value of best fit to LGM and PD states
Shallow ice approx. exponent, E_{SIA}	2.0, 3.0, 4.0*, 5.0	Non-linear effect	Non-linear effect	Decreases SC grounding-line extent	4.0
Shallow shelf approx. exponent, E_{SSA}	0.4, 0.6, 0.8*, 1.0	Decreases ice volume	Earlier retreat	Increases SC grounding-line extent	0.6
Sliding law exponent, q	0.25*, 0.5, 0.75, 1.0	Decreases ice volume	Later and more gradual retreat	Decreases SC grounding-line extent	0.5
Minimum till friction angle, Φ_{min} (°)	3, 4, 6, 9*	Increases ice volume	Later retreat	Prevents ice shelf collapse and improves SC grounding-line fit	9
Mantle viscosity, MV (Pa s)	1e18, 1e19*, 1e20, 1e21	Non-linear effect	Earlier and more rapid retreat, WAIS readvance at highest value	Increases SC grounding-line extent, grounds ice in WRS	1e19

the deglacial ice sheet evolution. Notably, the E_{SIA} parameter influences the grounded ice volume at LGM (Fig. 2), with a moderate value of 3.0 displaying the lowest ice volume as part of the WRS is unglaciated (Fig. 2b). With the exception of the outer WRS, the ice sheet grounding-line evolution through the Holocene is relatively consistent among the E_{SIA} experiments (Fig. 2a–d), resulting in similar present-day (PD) configurations (0 ka). Similarly to the E_{SIA} experiments, the E_{SSA} parameter results in differences in the outer WRS during the LGM (Fig. 3a–d). At the highest value of 1.0, the same region in the WRS is unglaciated at the LGM (Fig. 3d). Increasing E_{SSA} yields an earlier decline in grounded ice volume and ice shelf formation (Fig. 3e and f). The PD configuration also differs considerably among the experiments, with higher E_{SSA} values resulting in greater ice shelf area and lower grounded ice volume. The differences are observed along the Siple Coast. The best match to modern observation is found with E_{SSA} of 0.6, with lower (higher) E_{SSA} values underestimating (overestimating) the Siple Coast grounding line retreat.

The basal substrate terms of q and Φ_{min} are also consequential for the LGM and PD ice sheet configurations and response to deglacial climate forcing. Although the LGM grounding-line positions are relatively consistent among the q experiments, higher q leads to reduced grounding line extent along the Siple Coast by the end of the simulation (Fig. 4a–d). Although increasing q results in thinner ice over WAIS, the decline in grounded ice volume and increase in ice shelf area are delayed (Fig. 4e and f), with a range >2 ka between the experiments. In the Φ_{min} experiments, lower values result in reduced ice surface elevation over WAIS and open ocean area in the deep portion of the WRS due to reduced ice thickness of EAIS outlet glaciers (Fig. 5a–c). The decline in grounded ice volume and increase in ice shelf area occurs more gradually with decreasing Φ_{min} (Fig. 5e and f). At the lowest value of 3°, reduced buttressing due to ice shelf collapse leads to grounding line retreat beyond the modern day position in the PD configuration (Fig. 5a). At intermediate values (4° and 6°), minimum extent of the grounding line is overestimated along the southern Siple Coast and overestimated along the northern Siple Coast in the PD configuration (Fig. 5b and c).

The mantle viscosity term, which influences basal topography, is a key control on the LGM and PD end-member states and the ice sheet

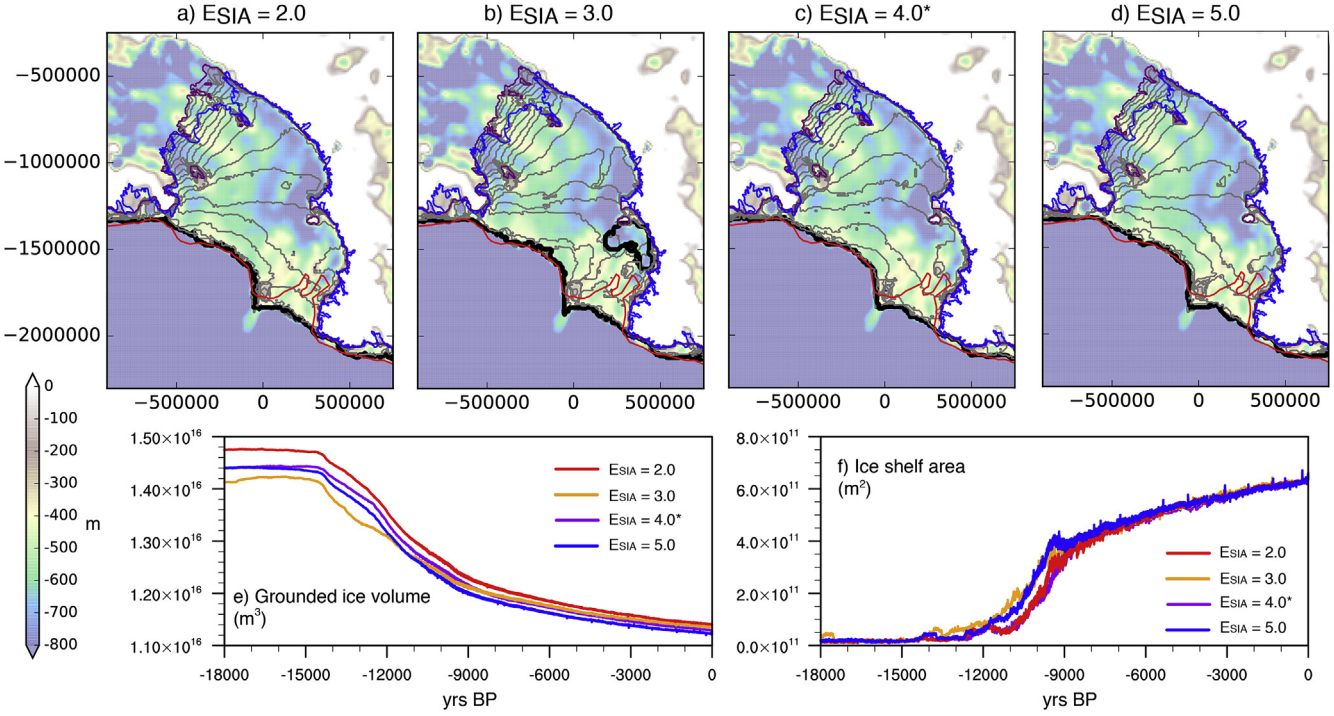

Fig. 2. Experiments varying the enhancement factor of the shallow ice approximation (E_{SIA}). (a–d) Grounding-line evolution, where the thick black line indicates modelled grounding-line position at the time of the glacial termination (18 ka), the gray lines indicate modelled grounding-line position every 1 ka, and the purple line indicates modelled grounding-line position at 0 ka. For comparison, the red line indicates the reconstructed LGM grounding line position, and the blue line indicates the modern grounding-line position. The asterisk indicates the standard value of E_{SIA}, and the experiment is the same as that shown in Fig. 1c. The grounding lines overlay the basal topography of 0 ka. (e) Modelled grounded ice volume (m^3) and (f) ice shelf area (m^2) evolution of the full model domain from 18 to 0 ka.

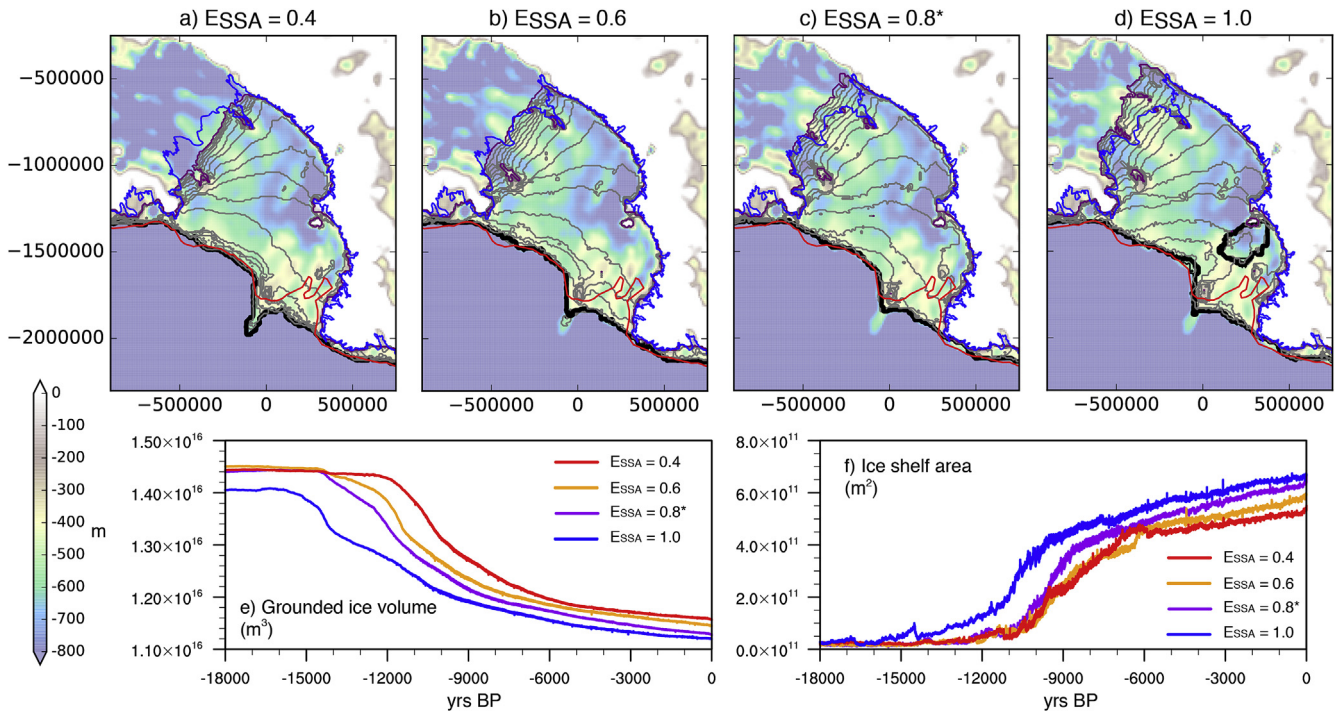

Fig. 3. Experiments varying the enhancement factor of the shallow shelf approximation (E_{SSA}). (a–d) Grounding-line evolution, where the thick black line indicates modelled grounding-line position at the time of the glacial termination (18 ka), the gray lines indicate modelled grounding-line position every 1 ka, and the purple line indicates modelled grounding-line position at 0 ka. For comparison, the red line indicates the reconstructed LGM grounding line position, and the blue line indicates the modern grounding-line position. The asterisk indicates the standard value of E_{SSA}, and the experiment is the same as that shown in Fig. 1c. The grounding lines overlay the basal topography of 0 ka. (e) Modelled grounded ice volume (m^3) and (f) ice shelf area (m^2) evolution of the full model domain from 18 to 0 ka.

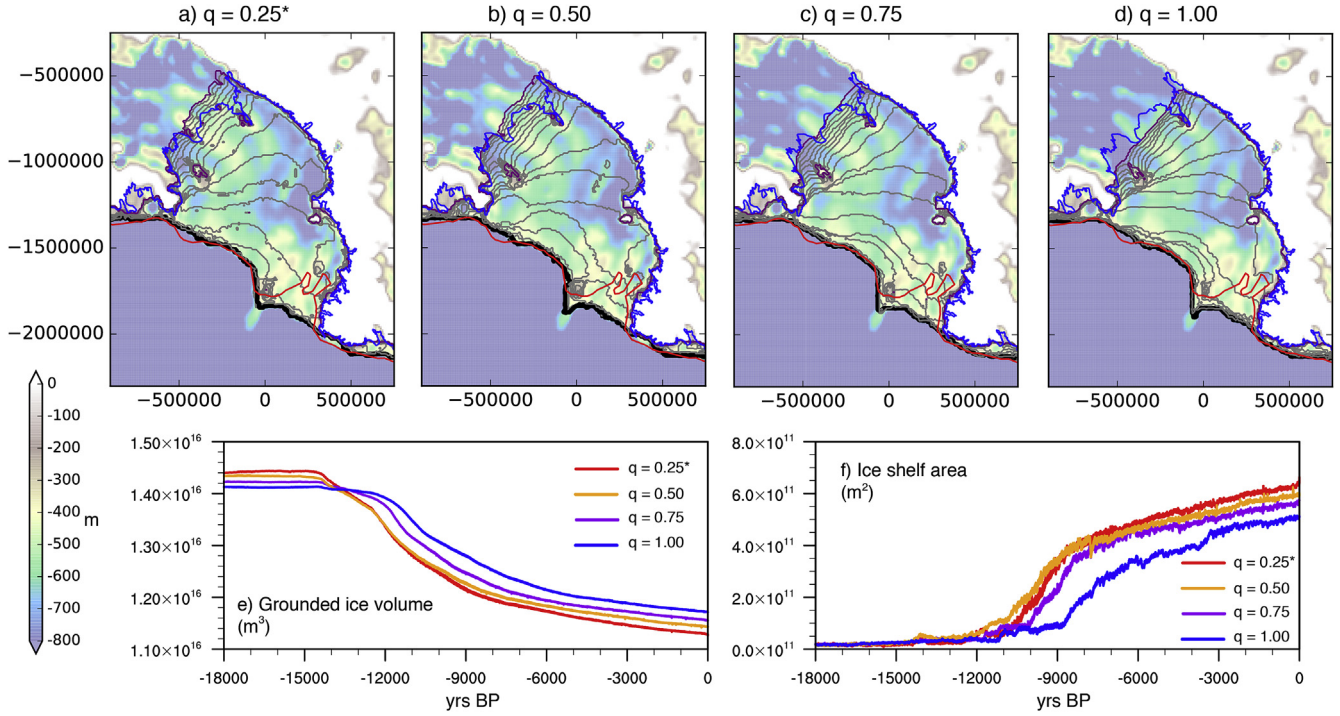

Fig. 4. Experiments varying the basal resistance parameter, q. (a–d) Grounding-line evolution, where the thick black line indicates modelled grounding-line position at the time of the glacial termination (18 ka), the gray lines indicate modelled grounding-line position every 1 ka, and the purple line indicates modelled grounding-line position at 0 ka. For comparison, the red line indicates the reconstructed LGM grounding line position, and the blue line indicates the modern grounding-line position. The asterisk indicates the standard value of q, and the experiment is the same as that shown in Fig. 1c. The grounding lines overlay the basal topography of 0 ka. (e) Modelled grounded ice volume (m^3) and (f) ice shelf area (m^2) evolution of the full model domain from 18 to 0 ka.

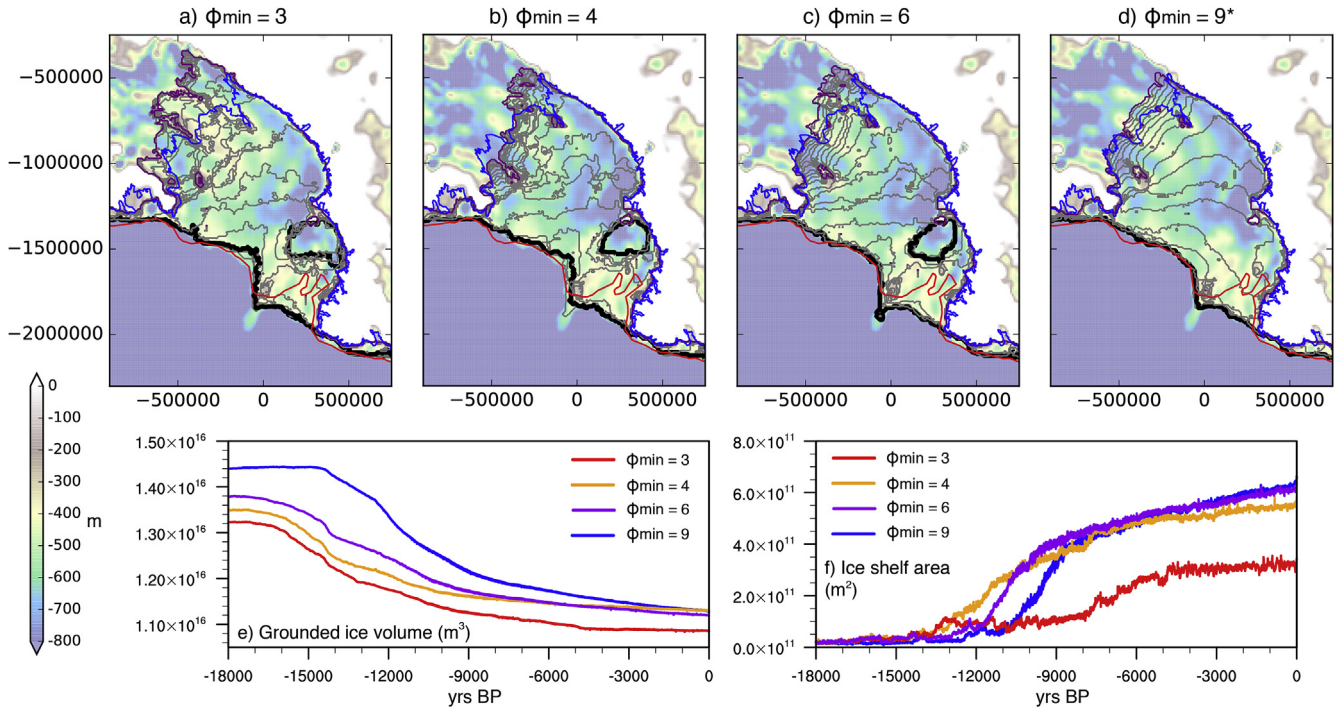

Fig. 5. Experiments varying the minimum till friction angle, Φ_{min} (°). (a–d) Grounding-line evolution, where the thick black line indicates modelled grounding-line position at the time of the glacial termination (18 ka), the gray lines indicate modelled grounding-line position every 1 ka, and the purple line indicates modelled grounding-line position at 0 ka. For comparison, the red line indicates the reconstructed LGM grounding line position, and the blue line indicates the modern grounding-line position. The asterisk indicates the standard value of Φ_{min}, and the experiment is the same as that shown in Fig. 1c. The grounding lines overlay the basal topography of 0 ka. (e) Modelled grounded ice volume (m^3) and (f) ice shelf area (m^2) evolution of the full model domain from 18 to 0 ka.

retreat history in this region. The highest mantle viscosity value of 1e21 Pa s results in considerably lower LGM ice volume due to the open ocean area in the WRS (Fig. 6d and e); this behavior is similar to the low Φ_{min} and high E_{SSA} experiments, as glacial advance is inhibited due to thinner EAIS outlet glaciers. The response to deglacial climate forcing is also more pronounced in the high mantle viscosity simulations (1e20 and 1e21 Pa s), with the grounding line retreating more rapidly and the ice shelf forming earlier, particularly in the 1e21 Pa s experiment. These simulations maintain higher ice shelf area through the Holocene, but only the experiment with a mantle viscosity of 1e21 Pa s displays WAIS readvance (~6 ka). The PD configuration of the 1e21 simulation overestimates grounding line extent along Siple Coast and a portion of the ice shelf in the WRS becomes grounded and the calving line does not match observations. In comparison, the lower mantle viscosity experiments show better agreement with the PD grounding-line position along the Transantarctic Mountains and Siple Coast as well as the calving line position.

If the Earth deformation scheme is not applied during the deglaciation, the ice sheet bed remains isostatically depressed and ice sheet retreat occurs rapidly between 14 and 11 ka (Fig. 7). Ice from both WAIS and EAIS becomes ungrounded in the early Holocene (by 11.4 ka). Propagation of retreat to the Transantarctic Mountains and the modern Siple Coast is completed by 11.2 ka, with the merging of ice shelf from the east and west into the main Ross Ice Shelf at this time. The grounding line continues to rapidly retreat on the WAIS side of the embayment over the next 1.2 ka, but the position remains fixed along the Transantarctic Mountains. Roosevelt Island becomes ungrounded ~10.4 ka. Over the last 10 ka of the simulation, the ice sheet shows relatively little change. The 0 ka configuration is consistent with the observed grounding line position along the Transantarctic Mountains and the modern calving line position. However, this simulation highlights the importance of isostatic rebound in the deglacial ice sheet evolution for the low-lying West Antarctic sector.

3.3. Spatiotemporal uncertainty due to model parameters and climate forcing

Among the four simulations of each parameter described in Section 3.2, the selection of Φ_{min} has the most significant impact on ice thickness through the deglacial period (Fig. 8a–e), followed by mantle viscosity and E_{SSA}. In comparison, the E_{SIA} simulations show relatively strong agreement in terms of ice thickness over this time interval. A substantial East-West trend is observed with increasing standard deviation from the Roosevelt Island region to the Ross Island region in nearly all sets of experiments. With the exception of q, each parameter shows relatively high ice thickness standard deviations (>400 m) in the WRS region. For q, the highest standard deviations (>200 m) are observed along the southern Siple Coast. The Φ_{min} simulations also exhibit high standard deviations over much of the modern Ross Ice Shelf and wider WAIS region (>400 m).

For the model parameter ensemble (17 simulations; the simulation with no bed deformation is not included), it is clear that the areas that are most sensitive to model parameter selection are the western Ross Sea, both to the north and south of Ross Island, and the southern Siple Coast (Fig. 8f). This is similar to the climate forcing model ensemble (39 simulations; Fig. 8g), which also shows the highest standard deviation of ice thickness in the WRS as compared to the ERS. However, it is notable that the standard deviations are relatively higher in Fig. 8f than in Fig. 8g, suggesting that the selection of model parameters tested in these simulations is more important in terms of the timing and pattern of ice sheet retreat than the selection of climate forcings. One reason for this is that there is a larger range of LGM and PD ice volumes in the model parameter ensemble versus the climate forcing ensemble. In contrast to the model parameter ensemble members, the end-member states of the climate forcing ensemble members are relatively consistent, hence the differences primarily result from differences in the timing of grounding line retreat.

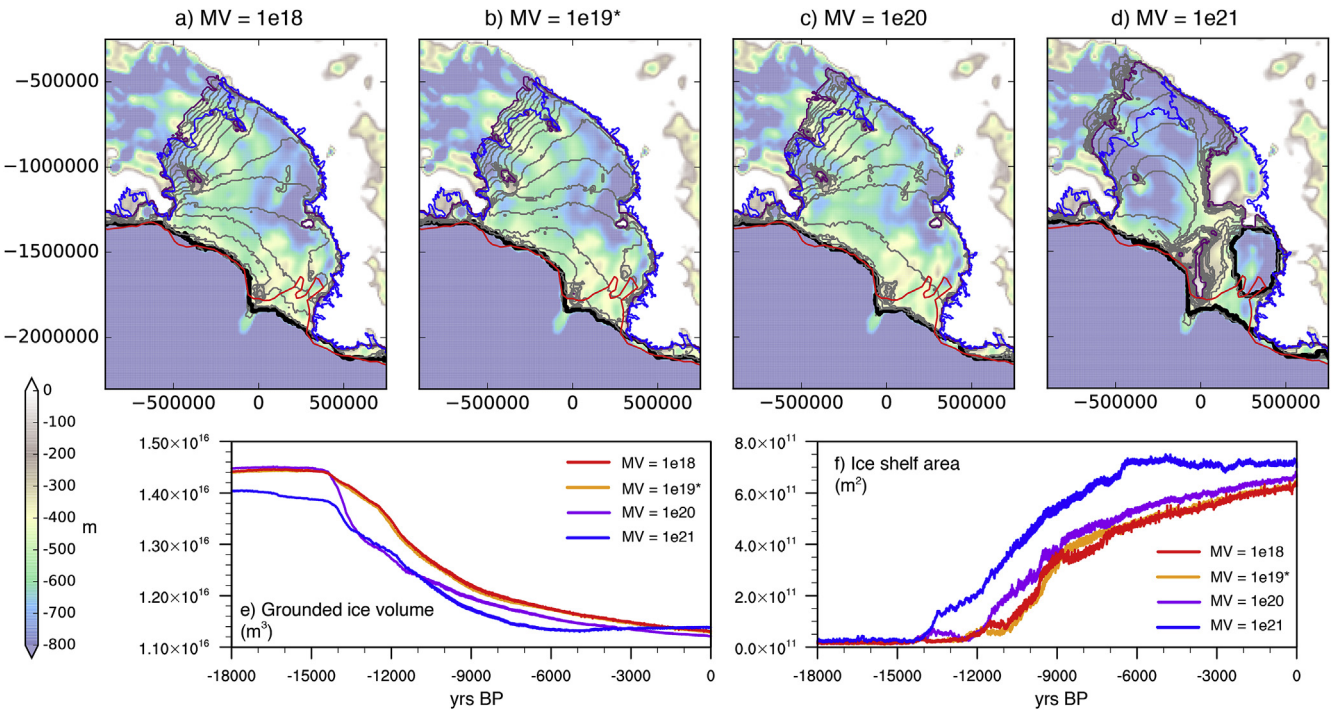

Fig. 6. Experiments varying the mantle viscosity (MV) term (units of Pa s). (a–d) Grounding-line evolution, where the thick black line indicates modelled grounding-line position at the time of the glacial termination (18 ka), the gray lines indicate modelled grounding-line position every 1 ka, and the purple line indicates modelled grounding-line position at 0 ka. For comparison, the red line indicates the reconstructed LGM grounding line position, and the blue line indicates the modern grounding-line position. The asterisk indicates the standard value of MV, and the experiment is the same as that shown in Fig. 1c. The grounding lines overlay the basal topography of 0 ka. (e) Modelled grounded ice volume (m^3) and (f) ice shelf area (m^2) evolution of the full model domain from 18 to 0 ka.

Considering both the climate forcing and model parameter ensembles together (i.e. 56 simulations in total), the standard deviation of ice thickness through the deglacial period demonstrates that the key area of uncertainty is the western Ross Sea, with standard deviation > 400 m to the north and south of Ross Island (Fig. 8h). Relatively high standard deviations also observed in the southern Siple Coast region and along the modern calving line. The WAIS catchment shows higher standard deviation than the EAIS catchment, though the ice streams of the Transantarctic Mountains show relatively high standard deviations. The model parameter ensemble contributes to the high standard deviations over the WAIS catchment, considering that the climate forcing ensemble shows relatively higher agreement in this region.

3.4. Comparison to EAIS and western Ross Sea proxy records

In nearly all model simulations, the grounded ice sheet reaches the continental shelf edge of the WRS at the LGM. Although the LGM grounding line position in this region is uncertain, some LGM reconstructions based on mapping of geomorphological features from multibeam swath bathymetry data suggest that much of the outer WRS remained ice free, with grounding-line embayments in the Drygalski, JOIDES, and Pennell Troughs (Domack et al., 1999; Shipp et al., 1999; Anderson et al., 2014; see red lines in Figs. 2–8). This ice sheet configuration more closely resembles the simulated ice sheet after the initial ice sheet retreat (~14–12 ka, depending on the climate scenario and model parameters), in which the ice sheet remains grounded on Pennell Bank, but is further retreated in the adjacent troughs. For the LGM, the models are more consistent with the view of Goehring et al. (2019), which shows that ice at the coast adjacent to the outer WRS thickened by several hundred meters at this time, implying that grounded ice probably extended at least as far as Tucker Glacier in Northern Victoria Land.

For the deglaciation, cosmogenic nuclide surface-exposure records of ice thinning at marginal sites in the Transantarctic Mountains provide the best estimates of ice thickness changes in the Ross Embayment. These records generally show enhanced thinning rates in the early-to-mid Holocene, although the precise timing differs among individual glaciers over a large time range of ~14–6 ka (Todd et al., 2010; Jones et al., 2015; Anderson et al., 2017; Spector et al., 2017; Goehring et al., 2019). As explained in Lowry et al. (2019a), comparisons between ice sheet model simulations and surface-exposure records are difficult due to limitations in model resolution, which may not be sufficient for resolving smaller-scale features, and reliable proxy data being sparsely distributed and having their own dating uncertainties. However, the parameter model experiments allow for analysis of which model parameters may contribute to the model-proxy discrepancies observed between regional ice thinning in the climate forcing model ensemble and individual glaciers. Here, we compare ice thickness changes of the model ensemble in three regions from which cosmogenic nuclide surface-exposure records exist: the Northern Transantarctic Mountain (NTAM) region, the McMurdo region, and the Southern Transantarctic region (STAM; Fig. 9).

Another model-proxy mismatch shown in Lowry et al. (2019a) is the difference in the timing and rate of ice thinning in the early Holocene, which occurs earlier in the model simulations than indicated in some of the surface-exposure records, particularly in the McMurdo region (Fig. 9b). It was argued that the bed smoothing parameterization contributed to this difference, as a rough bed would have more potential pinning points. Considering the abundance of ice rises in the western Ross Sea in particular (Simkins et al., 2016), this is an important consideration. The red lines in Fig. 9 show the effect of reduced bed smoothing (bed smoothing parameter decreased from 25e3 m to 10e3 m); although this higher bed roughness leads to increased glacial ice thickness, the rate of early Holocene ice thinning increases (Fig. 9a–c), in contrast to the previously proposed hypothesis. However, it should be noted that the bed in these simulations, which is based on the Bedmap2 dataset (Fretwell et al., 2013), is considerably smoother than reality even in the higher roughness simulation, hence uncertainty on its effect on ice sheet retreat remains.

Among the other model parameters tested, E_{SSA} shows the widest

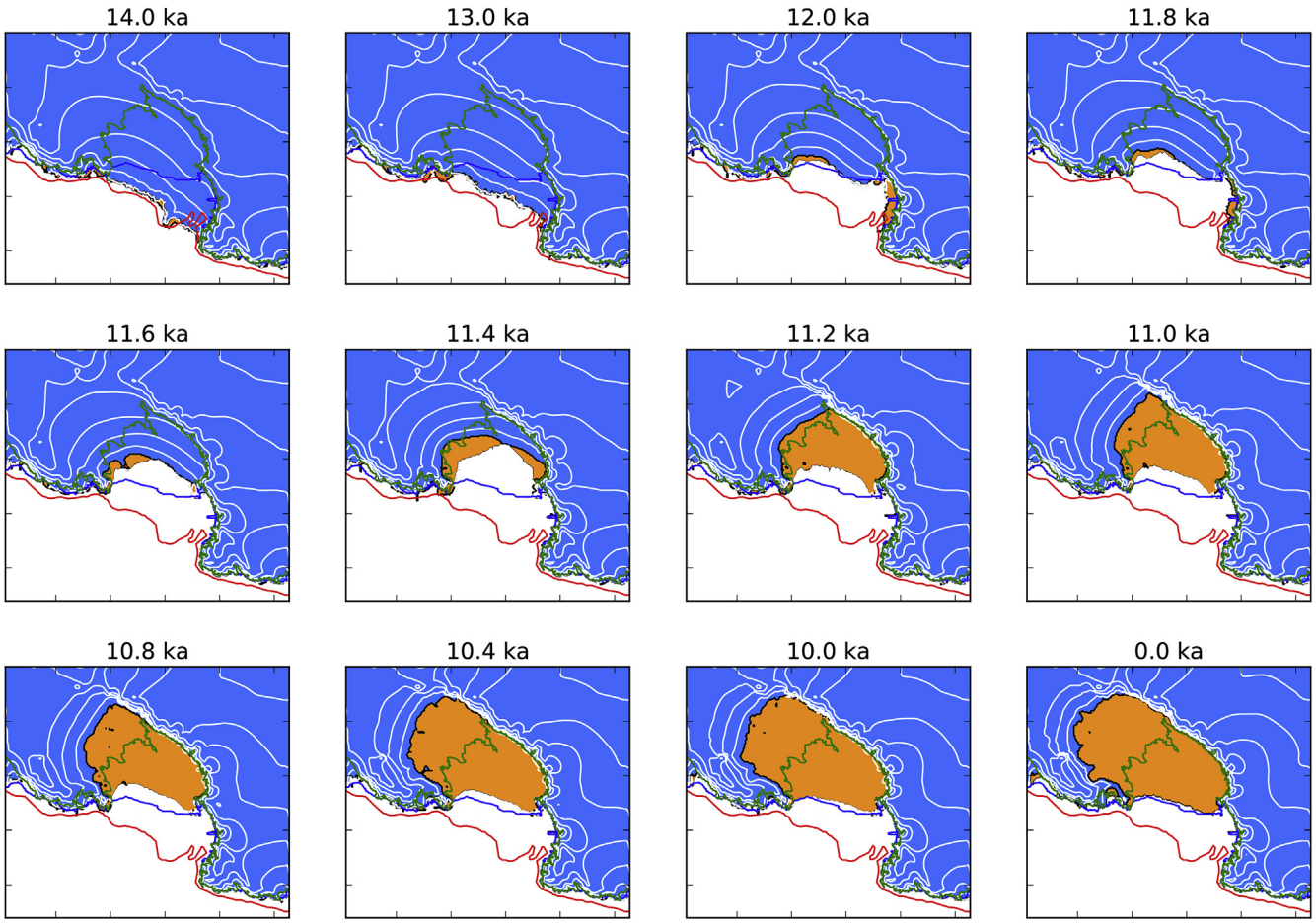

Fig. 7. Time slices of ice sheet evolution in the simulation with no isostatic rebound after 20 ka. As in the previous figures, blue indicates grounded ice, orange indicates floating ice, and the black line shows the modelled grounding line position. White lines denote surface elevation contours of 500 m. Observed grounding and calving line positions are shown in green and blue, respectively, and the estimated LGM ice sheet extent is shown in red.

range in ice thinning in the NTAM and McMurdo regions (brown lines in Fig. 9a and b). Using lower values of E_{SSA}, which reduces the velocity of ice streams and ice shelves, leads to higher glacial ice thickness and later ice thinning in these regions, whereas the reverse is true for the simulations that use higher E_{SSA} values. Although q does not show high standard deviation of ice thickness in this region (Fig. 8), higher q also yields a relatively later ice thinning, more consistent with Mt Discovery (purple lines in Fig. 9b), with an effect similar to cooler climate forcing. The mantle viscosity parameter has a substantial impact on ice thickness in both of the NTAM and McMurdo regions, with the highest value of 1e21 Pa s yielding very small changes in ice thickness; however, the mantle viscosity experiments display little variation in the STAM region (orange lines in Fig. 9). In contrast, low E_{SSA} (0.4) and high q (1.0) yield delayed retreat in the STAM region, more consistent with Scott Glacier (Fig. 9c). Reducing Φ_{min} (green lines), increasing q, and application of the WDC accumulation forcing (blue lines) produce lower glacial ice thickness in STAM, but still result in higher glacial ice thickness than estimated at Reedy Glacier.

The applications of cooler climate forcing, lower E_{SSA} values, and higher q delay the timing of grounding-line retreat in the WRS (Fig. 10). Some commonalities exist among the pattern of retreat, regardless of model parameter selection and climate forcing, highlighting the importance of seafloor bathymetry in driving the pattern of grounding line retreat, as argued in Halberstadt et al. (2016), McKay et al. (2016) and Lee et al. (2017). For example, each grounding line retreat evolution in Fig. 10 shows instances of grounding line stabilization from Pennell Bank, Crary Bank and Ross Island, with relatively rapid retreat occurring between these pinning points. However, differences are observed, with the simulation with q = 1.0 (i.e., sliding linearly related to the bed-parallel shear stress) displaying a more constant rate of retreat and no ice remaining grounded on Pennell and Crary Banks following ice sheet retreat. The other simulations (i.e., moderate climate, cool climate, and low E_{SSA}) are more consistent with the sequence of retreat suggested in the marine-based model of Halberstadt et al. (2016) based on interpretation of the geomorphic features of the seafloor. Retreat over Ross Bank is relatively consistent among the simulations, with no substantial grounding-line stabilization occurring, unlike Pennell and Crary Banks. This may be related to differences in elevation between the three features, with Ross Bank lying ~140 m below Pennell Bank and ~120 m below Crary Bank. No model simulation captures the mid-Holocene EAIS readvance proposed by Greenwood et al. (2018) for the McMurdo region, indicating that this is a local signal that the model is incapable of resolving, or that the climate forcing (i.e., precipitation and ocean forcing) is inadequate for this region.

3.5. Comparison to WAIS deglacial reconstructions

Reconstruction of surface elevation change in WAIS is more difficult than in the Transantarctic Mountains considering the lack of surface-exposure records. Those that do exist are from marginal sites of Marie Byrd Land and show a wide range of surface elevation changes ranging from the early to late Holocene. For example, surface-exposure ages from glacial deposits in the Ford Ranges of Marie Byrd Land suggest ~700 m of continuous ice thinning since 10 ka Stone et al.,(2003). In contrast, dated glacial erratics of the Ohio Range and Mt Waesche possibly indicate highstands in ice sheet elevation of ~100 m and ~60 m at 10 ka,

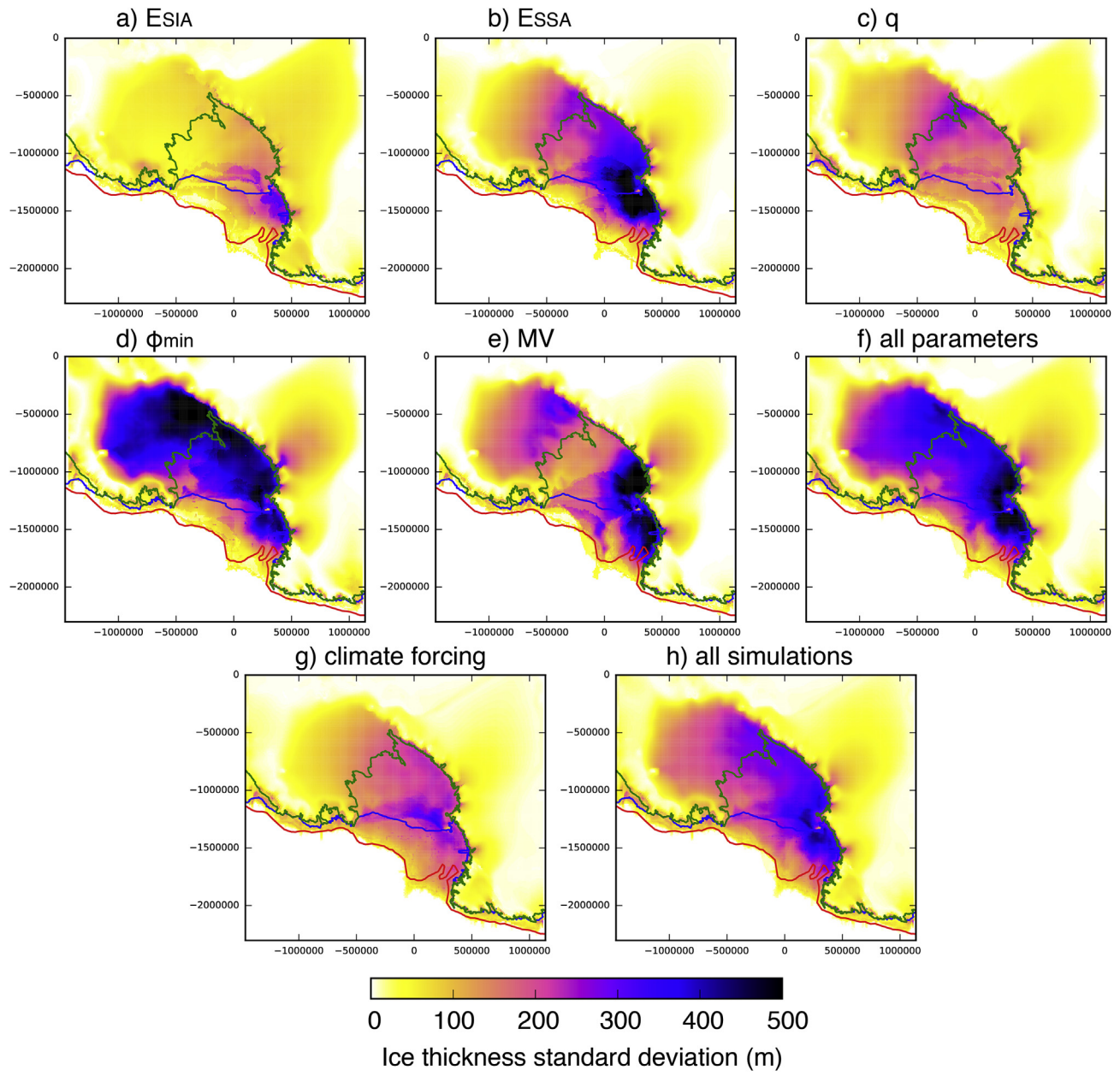

Fig. 8. (a–e) Time-averaged standard deviation of ice thickness (m) for the period of 18 to 4 ka in experiments varying a single model parameter, i.e., enhancement factors of SIA and SSA (E_{SIA} and E_{SSA}, respectively), basal resistance (q), till friction angle (Φ_{min}), and mantle viscosity (MV). The standard deviation of ice thickness among each set of experiments was calculated for each model grid cell at 1000 year increments and then averaged for the period of 18 ka to 4 ka. (f) Time-averaged standard deviation of ice thickness of all experiments from panels a–e (17 simulations total; the simulation without bed deformation is not included). (g) Time-averaged standard deviation of ice thickness of the climate forcing ensemble (39 simulations total). (h) Time-averaged standard deviation of ice thickness of all experiments in panels a–e and g (56 simulations total).

respectively (Ackert et al., 2013). Attempts have also been made to estimate changes in surface elevation in the WAIS interior through the deglacial period from a modeling perspective. Continental-scale climate-forced ice sheet model simulations have produced LGM ice thickness changes ranging from <50 m to 360 m at WAIS Divide (Pollard and DeConto, 2009; Golledge et al., 2014; Pollard et al., 2015). The ICE-5G and ICE-6G glacial isostatic adjustment model scenarios, generally used in climate model simulations, suggest larger ice thickness changes of WAIS through the deglacial period (Peltier, 2004; Argus et al., 2014). Given the wide range of estimates and evolving nature of interpretations, high uncertainties of WAIS ice thickness changes remain.

At WAIS Divide, the climate forcing model ensemble shows LGM surface elevation changes of ~200 m, within the range of the above-mentioned continental-scale ice sheet model simulations, but below the ICE-5G and ICE-6G estimations (Fig. 11a). The climate forcing model ensemble members are also generally consistent with the modern WAIS Divide surface elevation of 1797 m. Increasing q and decreasing Φ_{min} reduces the LGM ice surface elevation (purple and green lines in Fig. 11a, respectively), and in the simulations with lower Φ_{min}, the modern surface elevation is underestimated. Other outliers from the model parameter ensemble members include the simulation with E_{SSA} of 0.4 (brown line in Fig. 11a), in which the total deglacial change is ~80 m and the modern surface elevation is overestimated by 140 m, and the simulation with mantle viscosity of 1e21 Pa s (orange line in Fig. 11a), which is the only

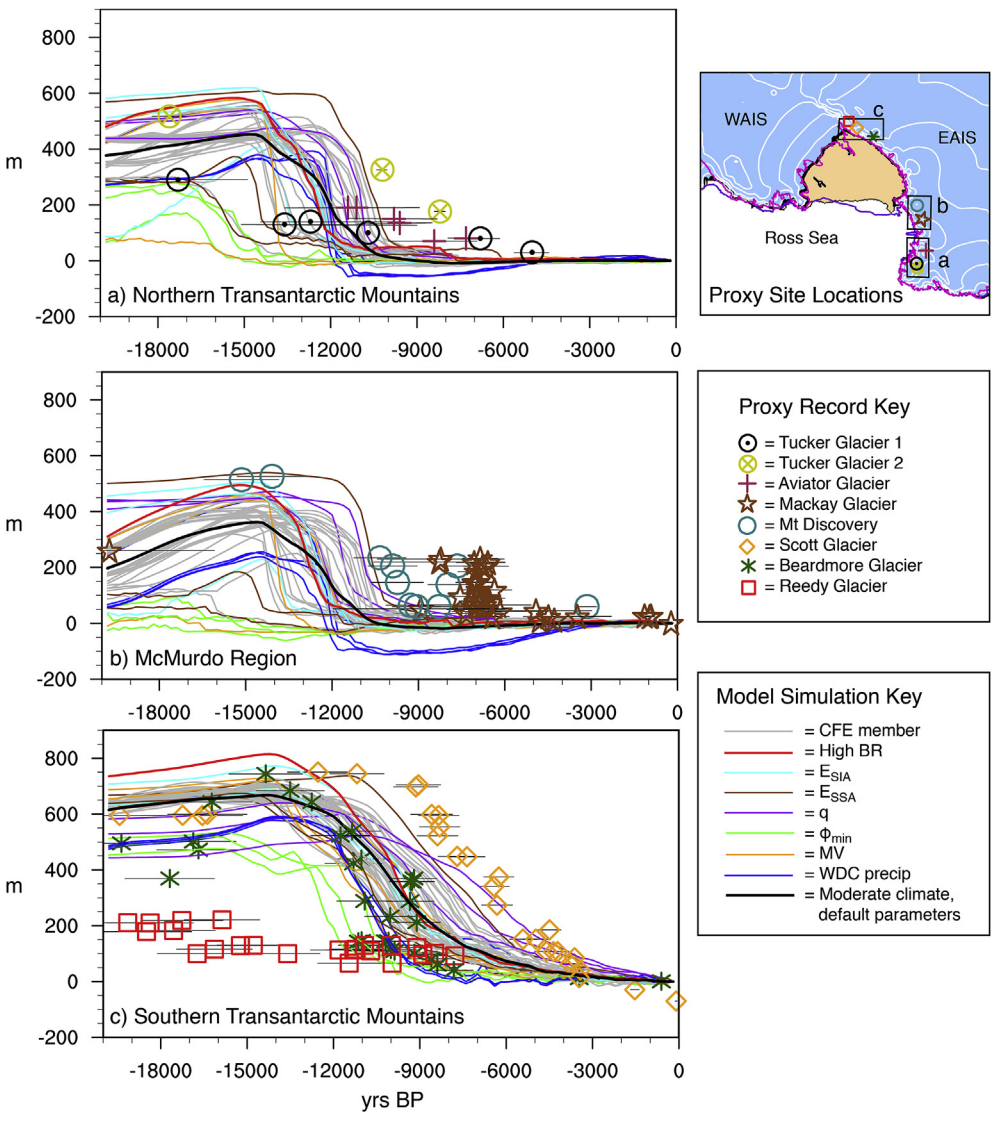

Fig. 9. Regional ice thickness anomalies relative to PD of the model simulations for the (a) NTAM, (b) McMurdo, and (c) STAM regions vs. ice thickness anomalies of cosmogenic nuclide surface-exposure records of glaciers within each region. Climate forcing ensemble (CFE) members are shown in gray, with the exception of the moderate climate forcing scenario from Fig. 1 shown in black. The cyan and brown lines show the E_{SIA} and E_{SSA} experiments, respectively. The purple, green and red lines show the q, Φ_{min}, and bed roughness (BR) experiments, respectively. The orange lines show the mantle viscosity experiments. The blue lines show the experiments using the WDC accumulation record as precipitation forcing. The NTAM glacier data were obtained from Goehring et al. (2019). Data for Mt Discovery and Mackay Glacier were obtained from Anderson et al. (2017) and Jones et al. (2015), respectively. The STAM glacier data were obtained from Spector et al. (2017) and Todd et al. (2010). All exposure ages were recalculated following recent improvements to global production rate (Borchers et al., 2016). Age uncertainties of the records are indicated by the horizontal bars. The map to the right of the panels shows the glacier locations overlaid on the ensemble average of the final modelled RIS configuration (yellow shows floating ice, blue shows grounded ice, thick black line shows modelled grounding-line position, white contours show surface elevation in 500 m intervals, pink line shows observed modern grounding-line position, and purple line shows observed modern calving line position). The black boxes indicate the regions used for the regional averages (in WGS84 Antarctic Polar Stereographic x,y coordinates): NTAM (400000–500000 x, −1900000 — -1600000 y), McMurdo (400000–550000 x, −1450000 — -1300000 y) and STAM (-225000 — 97500 x, −625000 — -375000 y).

one showing decreasing surface elevation in the early Holocene (~11.8 ka) and isostatic rebound-driven increase in surface elevation in the late Holocene. The relative change of this simulation with high mantle viscosity is similar to the ICE-5G and ICE-6G estimations, but the modelled surface elevation is lower through this interval and the modern surface elevation is slightly underestimated (<100 m).

Downstream of the western WAIS Divide, the difference between the ICE-5G and ICE-6G estimations is more significant in terms of the LGM WAIS surface elevation. The model simulations generally producing higher LGM surface elevations than ICE-6G and lower LGM surface elevations than ICE-5G at Siple Dome and Roosevelt Island (Fig. 11b and c). Similar to WAIS Divide, the outliers of the model parameter ensemble include the Φ_{min}, q, E_{SSA} and high mantle viscosity experiments (green, purple, brown, and orange lines, respectively). Decreasing Φ_{min} improves the model fit to ICE-6G estimations at Siple Dome, whereas increasing q leads to higher-than-observed modern ice surface elevation at this site (Fig. 11b). At Roosevelt Island, decreasing Φ_{min} also yields an LGM surface elevation that is more consistent with ICE-6G, but the high q, low E_{SSA} and cool climate forcing simulations, which produce a delayed ice sheet retreat, are more consistent with the timing of the ICE-6G decrease (Fig. 11c). The high mantle viscosity simulation shows a rapid decrease in ice surface elevation at both sites in response to ocean thermal forcing at ~14 ka.

In terms of the grounding-line evolution along the Siple Coast, the moderate climate forcing simulation shows a southwestward propagation of the grounding line from Roosevelt Island and Crary Ice Rise through the mid-to-late Holocene (Fig. 12a). The grounding-line position at 0 ka is consistent with modern observations along the northern Siple Coast (i.e., MacAyeal and Bindschadler ice streams), but retreat is overestimated to the south. Application of cool ocean forcing and WDC-derived precipitation forcing, which is higher through the Holocene, improves the fit to modern observations of grounding-line position (Fig. 12b). Although decreasing Φ_{min} yields an ice surface elevation evolution at Siple Dome that is more consistent with ICE-6G, the simulation with Φ_{min} of 4 shows overestimated grounding-line retreat of the southern Siple Coast by 7 ka, and underestimated grounding-line retreat of the northern Siple Coast by 0 ka (Fig. 12c). Mantle viscosities above 1e20 Pa s are required for the WAIS retreat-readvance scenario proposed by Kingslake et al. (2018). With mantle viscosity of 1e21 Pa s, the readvance initiates by 6 ka, later than the 5e20 simulation discussed in Lowry et al. (2019a), but the grounding-line extent at 0 ka still overestimates modern observations (Fig. 12d).

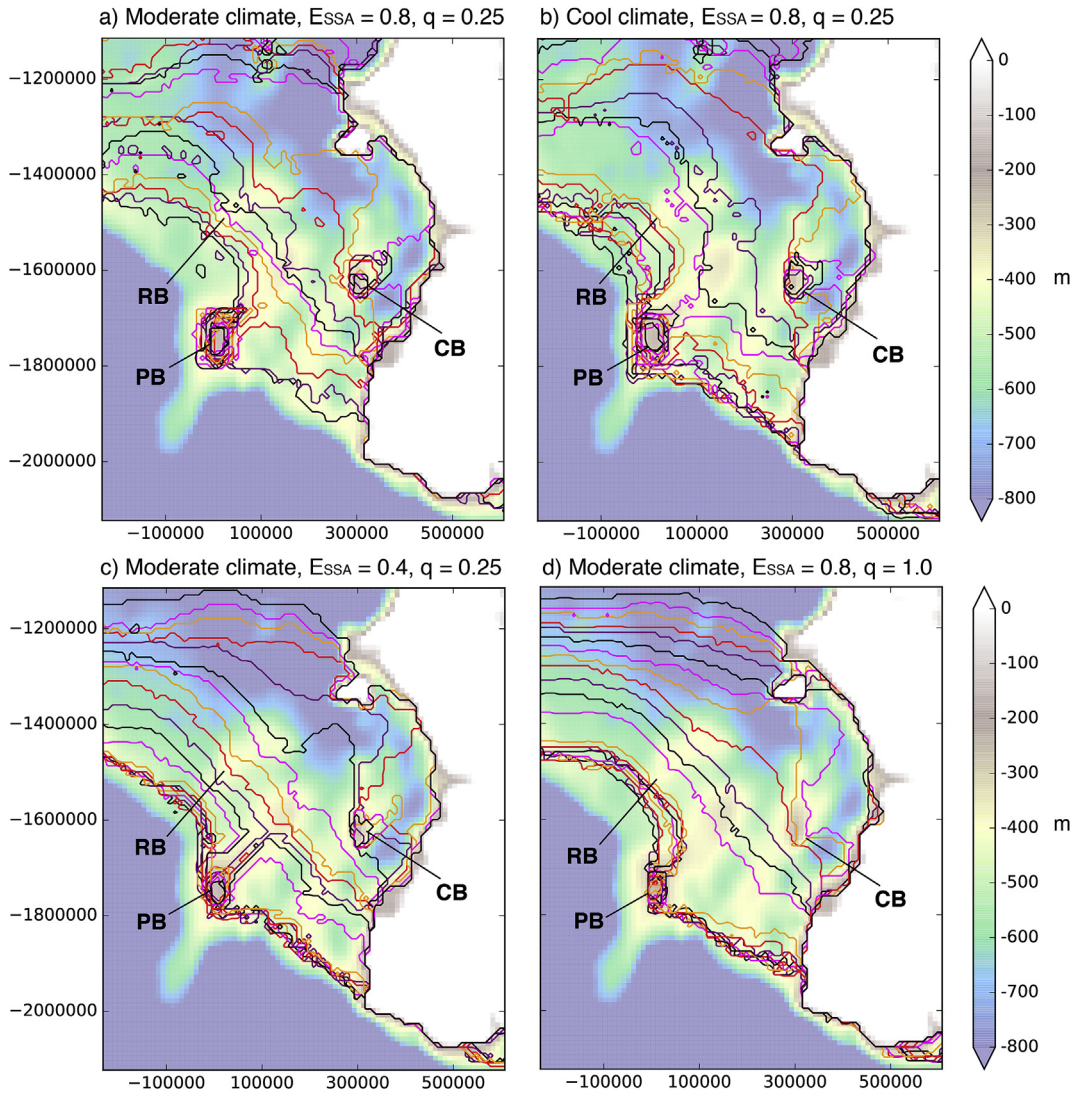

Fig. 10. Changes in grounding-line position in the Western Ross Sea for the period of 14 to 10 ka for the following simulations: (a) the moderate climate forcing with standard model parameters (same as Fig. 1c), (b) cool climate forcing with standard model parameters (same as Fig. 1b), (c) E_{SSA} of 0.4, and (d) q of 1.0. Black lines indicate grounding-line position for periods of 1000 years, whereas coloured lines indicate 200-yr grounding-line changes with the sequential order of purple, red, orange, pink. The grounding lines overlay modelled basal topography at 10 ka. Locations for Ross Bank (RB), Pennell Bank (PB), and Crary Bank (CB) are indicated.

4. Discussion

4.1. Model sensitivity to parameters and climate forcing

Of the model parameters examined here, Φ_{min}, mantle viscosity, and E_{SSA} show the greatest influence on the broader-scale ice sheet sensitivity to climate forcing. As the Φ_{min} parameter increases, the LGM ice thickness increases, and the ice sheet becomes less sensitive to deglacial climate forcing. In comparison, the E_{SSA} experiments show less variation in terms of the LGM configuration, but increasing E_{SSA}, which enhances ice shelf and ice stream velocity and basal sliding, yields higher sensitivity to climate forcing. Increasing mantle viscosity causes the ice sheet to respond more rapidly to climate forcing, but the retreat-readvance scenario described in Kingslake et al. (2018) is only reproduced with mantle viscosity >1e20 Pa s, which is consistent with their findings. Although the E_{SIA} and q parameters show relatively less influence on ice sheet retreat behavior, E_{SIA} does impact the LGM ice thickness, and increasing q, which increases basal resistance, delays the ice sheet response to climate forcing, as expected.

Within the model domain, these model parameters may contribute to the differences in the local grounding-line retreat and ice thinning behavior observed in proxy records and reconstructions of different locations. For example, Halberstadt et al. (2016) proposes an asynchronous pattern of grounding-line retreat between the ERS and WRS. This is generally confirmed in comparing available WAIS radiocarbon ages (McKay et al., 2016; Bart et al., 2018; Kingslake et al., 2018) with surface-exposure records of the Transantarctic Mountains (Jones et al., 2015; Anderson et al., 2017), which suggest a later WRS retreat and delayed ice thinning of EAIS outlet glaciers. While it is difficult to determine how differences in climate forcing and ocean circulation influenced this pattern of retreat, we show here that geological and glaciological factors cannot be discounted as controls. In particular, the relatively low mantle viscosity of the WRS likely reduced the ice sheet response to climate forcing as compared to the ERS, which has a higher mantle viscosity (Whitehouse et al., 2019). The spatial heterogeneity of this parameter therefore poses a significant challenge in modeling the embayment-scale retreat pattern and requires consideration in comparing individual model simulations to proxy records. The implications of this are discussed in greater detail in the subsequent sub-sections with regard to WRS versus ERS retreat.

Despite the importance of the individual model parameters, the influence of the climate forcings in deglacial retreat should not be

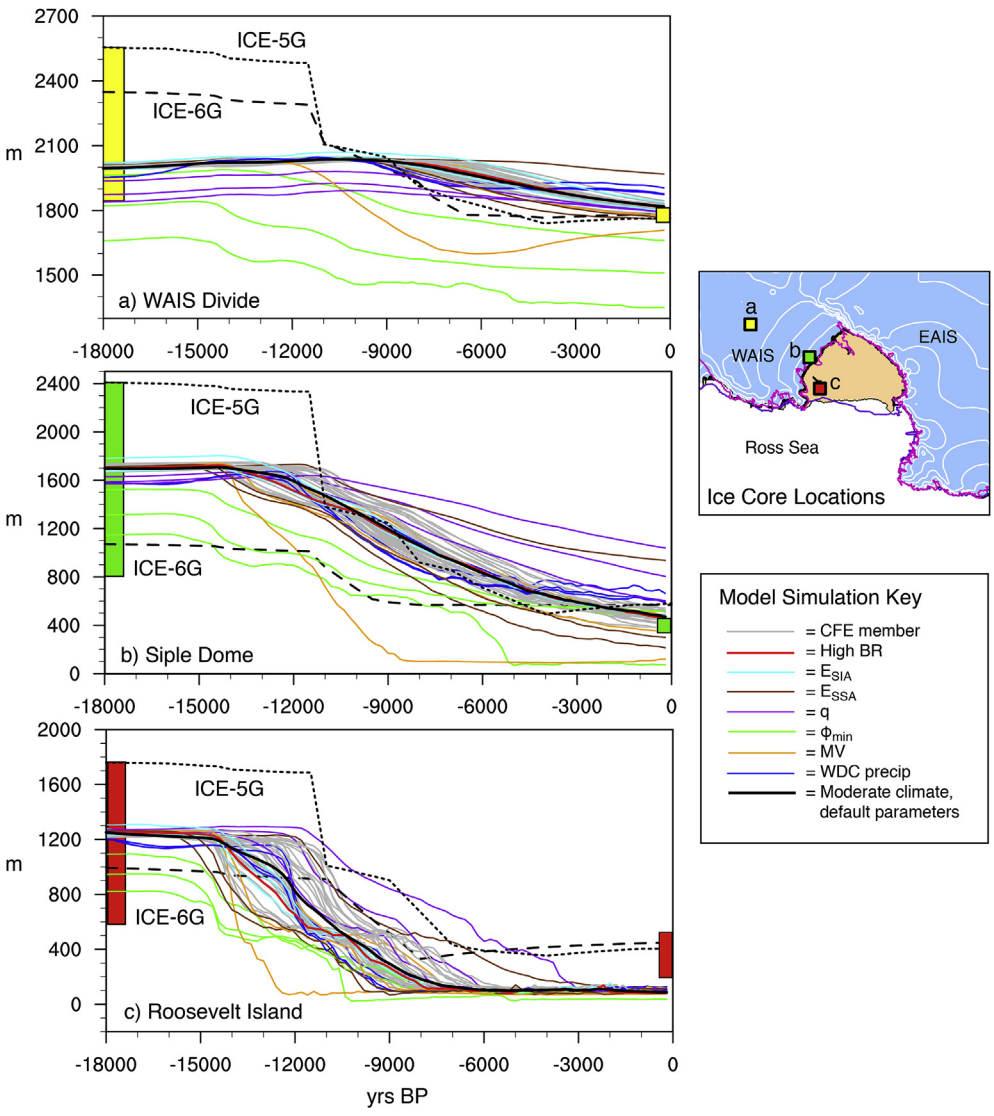

Fig. 11. Modelled ice surface elevation at (a) WAIS Divide, (b) Siple Dome, and (c) Roosevelt Island compared to ICE-5G and ICE-6G reconstructions (Peltier, 2004; Argus et al., 2014). Climate forcing ensemble (CFE) members are shown in gray, with the exception of the moderate climate forcing scenario from Fig. 1 shown in black. The cyan and brown lines show the E_{SIA} and E_{SSA} experiments, respectively. The purple, green and red lines show the q, Φ_{min}, and bed roughness (BR) experiments, respectively. The blue lines show the experiments using the WDC accumulation record as precipitation forcing. ICE-5G and ICE-6G are indicated by the small and large dashes, respectively. Locations of these ice core sites are shown in map to the right of the panels, i.e., the ensemble average of the final modelled RIS configuration (yellow shows floating ice, blue shows grounded ice, thick black line shows modelled grounding-line position, white contours show surface elevation in 500 m intervals, pink line shows observed modern grounding-line position, and purple line shows observed modern calving line position).

understated in these simulations. In particular, the sub-ice shelf melt rate and back pressure forcings are scaled to ocean and air temperature, respectively; the scaling relationships were determined from a suite of sensitivity experiments described in Lowry et al. (2019a). In these experiments, if the scaling relationships for the sub-ice shelf melt rate and back pressure forcings are too low, the grounding-line retreat is insufficient, and if they are too high, the ice shelf collapses. Only a narrow range of LGM anomalies successfully reproduces a glacial advance to LGM estimates of grounding-line position with a retreat to a near-modern grounding-line position and accurate calving line (Lowry et al., 2019a). Although this is one method of ocean forcing, it should be noted that the conversion of temperature to sub-ice shelf melt rate parameterization is complex and an active area of research in the ice sheet model community (Pattyn et al., 2017). While coupling to models that simulate ice shelf cavity circulation can improve accuracy (e.g., Seroussi et al., 2017), this is currently impractical for simulations of this time scale. In addition to the importance of circulation, which is not considered here, the results of this study highlight the need to better understand ocean forcing in the context of model parameters related to basal substrate, bed deformation and ice flow.

4.2. Controls on ice sheet retreat in the Western Ross Sea

Mantle viscosity is a key parameter influencing the isostatic response of the solid Earth to the growth and decay of the Antarctic ice sheet, and thus is an important consideration for modeling deglacial ice sheet retreat the Ross Sea region (McKay et al., 2016; Kingslake et al., 2018). Although the climate forcing ensemble uses a low mantle viscosity (1e19 Pa s), consistent with the WRS, the majority of model simulations show earlier ice thinning than surface-exposure records from Mackay Glacier and Mt Discovery (Jones et al., 2015; Anderson et al., 2017). Simulations that use cool atmosphere and ocean forcings, which show delayed WRS grounding-line retreat, are more consistent with these records. Additionally, reducing E_{SSA} and increasing q also delay ice thinning in the Southern Victoria Land region. Using an E_{SSA} of 0.4 reduces the ice shelf velocity and allows the temporary ice shelf that fringes the EAIS outlet glaciers in the early Holocene to last for a longer duration. Although a q of 1.0 also delays WRS grounding-line retreat, the retreat pattern is inconsistent with the sequence of retreat described in Halberstadt et al. (2016), as no ice remains grounded on Pennell and Crary Banks following ice sheet retreat. These models therefore suggest that the rheological properties and flow velocities of EAIS-derived ice, as they relate to E_{SSA}, and climate forcing are the relevant controls to focus on in improving the model-data fit in this region.

The main area of uncertainty in both the climate forcing and model parameter ensembles is the WRS. In the case of the climate forcing ensemble, this is related to the variation in the timing of grounding-line retreat as simulations forced with relatively warmer atmosphere and

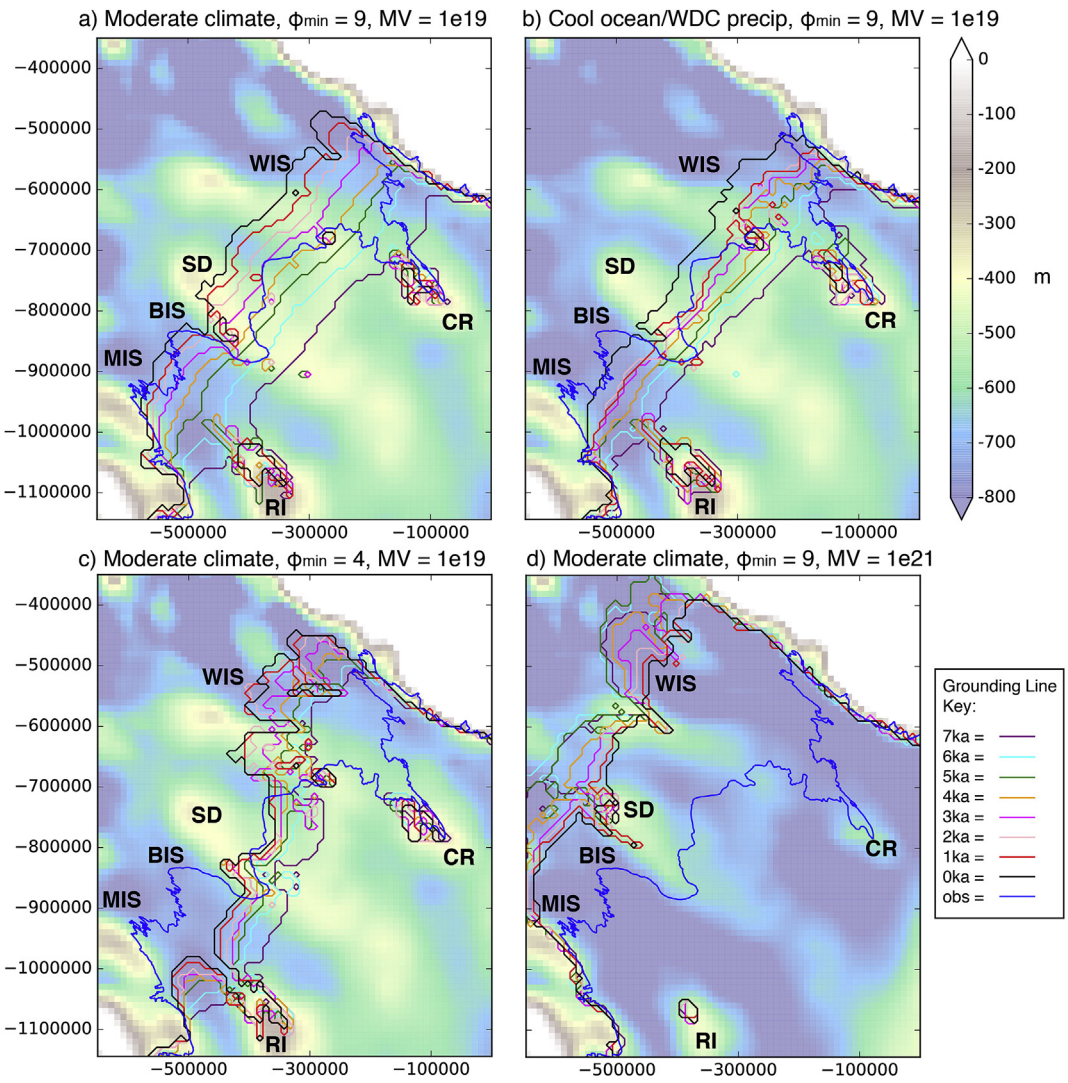

Fig. 12. Modelled changes in grounding-line position along the Siple Coast for the period of 7 to 0 ka for the following simulations: (a) the moderate climate forcing with standard model parameters (same as Fig. 1c), (b) cool climate forcing and WDC precipitation forcing, (c) Φ_{min} of 4, and (d) MV of 1e21 Pa s. The blue line indicates the observed grounding line position (obs). The grounding lines overlay modelled basal topography at 0 ka. Locations for Roosevelt Island (RI), Siple Dome (SD), Crary Ice Rise (CR), MacAyeal Ice Stream (MIS), Bindschadler Ice Stream (BIS), and Whillans Ice Stream (WIS) are indicated.

ocean forcings retreat approximately 2 ka earlier than those forced with relatively cooler atmosphere and ocean forcings (Lowry et al., 2019a). In the case of the model parameter ensemble, the high standard deviation of the simulations in this region is also related to the glacial configuration of the ice sheet, in which adjustments of E_{SIA}, E_{SSA}, Φ_{min}, and mantle viscosity lead to the inhibition of ice flux of Transantarctic outlet glaciers. This common response among the simulations, which results in an area of the WRS remaining unglaciated, may be indicative of an issue with model resolution. The region also has a tectonic history that may be especially difficult to reproduce in model simulations; for example, the East Antarctic side of the tectonic boundary in the Ross Sea has a thinner crust, and thus experienced a greater amount of extension than the West Antarctic crust (Behrendt and Cooper, 1991; Tinto et al., 2019). This is not accounted for in the mantle viscosity experiments. In addition, improvements to the representation of local-scale bed topography from the Bedmap2 dataset could also be critical for simulating local ice dynamics of the Transantarctic outlet glaciers.

Another outstanding issue in Southern Victoria Land is the early Holocene (~8.5 ka) ice sheet readvance proposed by Greenwood et al. (2018). The proposed readvance was significant enough for the grounding-line to potentially reach as far as Joides Trough, but none of the model simulations reproduce this behavior. Greenwood et al. (2018) attribute the readvance to flow-switching and enhanced flow velocity associated with the unzipping of ice sheet sub-sectors as the grounding line retreated toward the South Victoria Land outlet glaciers, and also suggest that an increase in precipitation, related to the increased available moisture from the open ocean, may have occurred. The model simulations may fail to reproduce this advance due to the above-mentioned limitations in model resolution, which may inadequately represent the local-scale ice dynamics involved in this flow-switching behavior, and in the precipitation forcing, which does not increase substantially through this interval (see Lowry et al., 2019a).

Ocean circulation may also be an important element to this EAIS readvance and other model-proxy discrepancies in the WRS as the ocean cavity beneath the Ross Ice Shelf begins to form. Sub-ice shelf melt becomes the primary control of ice sheet retreat as the ocean cavity underneath the developing Ross Ice Shelf expands starting in the early Holocene, but a local ice shelf fringing the EAIS outlet glaciers is also present at this time (Lowry et al., 2019a). Meltwater flux from enhanced basal melting of the developing Ross Ice Shelf in the mid-Holocene may have increased marine ice formation of the local EAIS ice shelf, similar to the modern process of sea ice stabilization from the ice shelf cavity freshwater flux observed in the WRS (Hellmer, 2004). The seafloor bathymetry and surface winds, which influence ocean circulation below the

ice shelf, also lead to interbasin differences in melt rates by controlling incursions of water masses from the Ross Sea, including relatively warm mCDW and relatively cool High Salinity Shelf Water (HSSW) (Dinniman et al., 2018; Tinto et al., 2019). Since the ocean thermal forcing applied in these simulations neglects ocean circulation, such ice-ocean interactions and feedbacks and spatial heterogeneity in sub-ice shelf melt rates are lacking, which may also account for the model-data mismatch.

In Northern Victoria Land, the Tucker and Aviator Glacier records exhibit a similar timing in the initial ice thinning, but show a more gradual decrease than the model simulations. It is important to note that these glaciers are not connected to the EAIS, have higher accumulation than further inland, and are located in an area of rough alpine topography (Baroni et al., 2005); as a result, they may not be reflective of the regional deglacial ice sheet evolution of North Victoria Land. Goehring et al. (2019) highlight the similarity between the ice thinning chronologies of the glaciers and global sea level, however, sea level forcing alone cannot account for ice sheet retreat in these ice sheet model simulations. Ocean and atmosphere forcing are the primary controls, though sea level forcing does enhance their effect. The discrepancy in rate may partially be accounted for by the E_{SSA} term, which can be adjusted to show better agreement to both glaciers, and increasing bed roughness, which stabilizes the ice thickness in this region following the initial decrease.

Lastly, the back pressure forcing, which is intended to mimic the stabilizing effect of dense sea ice, may decrease too dramatically in the early Holocene. The back pressure forcing is derived from a scaling relationship of ice core surface temperature records and modelled surface temperature of deglacial climate simulations. As a result, the forcing may be impacted by a decrease in ice surface elevation that may partially account for the temperature increase in the early Holocene in the ice core records, and in one of the climate models (see Lowry et al., 2019b). A back pressure forcing scaled to modelled or reconstructed sea ice concentration or thickness may decrease more gradually through the early Holocene and improve the model fit to the surface-exposure data of North Victoria Land.

4.3. Controls on ice sheet retreat in the Eastern Ross Sea

For WAIS, the most influential parameter examined here is Φ_{min}. Decreasing Φ_{min} reduces the LGM surface elevation and causes earlier ice sheet retreat and ice shelf formation. At the specific sites of Siple Dome and Roosevelt Island, the simulations with lower Φ_{min} show better agreement with the ICE-6G estimations of Argus et al. (2014), however, these simulations are least consistent at WAIS Divide. Φ_{min} is related to the material properties of the till, and although this term becomes spatially variable through its relationship to bed elevation (Equation 3), it is difficult to determine a Φ_{min} value that improves model fit in each part of the model domain. Till deformation has been shown to be an important control on WAIS-derived ice stream flow (Alley et al., 1986; Hulbe et al., 2016). Considering the proximity of Roosevelt Island and Siple Dome to these ice streams, accurate reconstruction of their surface elevation may depend on adequate representation of the till properties in ice sheet models. Here, we focus on Φ_{min}, but the bed elevation terms and Φ_{max} are also important components in τ_c. Future work should explore the influences of each component as it relates to the WAIS-derived ice streams.

The other parameter likely driving differences between WAIS and EAIS evolution and grounding-line retreat in the ERS and WRS is the previously discussed mantle viscosity term, which is higher in the ERS (Whitehouse et al., 2019). This may in part explain the early retreat indicated in marine radiocarbon ages in the Whales Deep Basin (Bart et al., 2018), as the high mantle viscosity (>1e20) could have made the ice sheet more sensitive to sub-surface ocean warming resulting from melting of the Antarctic Peninsula and the mid-to-outer Weddell Sea (Golledge et al., 2014). The simulations with higher increases in Meltwater Pulse 1a-associated sub-shelf melt rates in Lowry et al. (2019a) are consistent with the early retreat timing of Bart et al. (2018), as are those with mantle viscosity ≥5e20 Pa s. However, the scenario of Bart et al. (2018) also indicates a grounding-line stabilization on the outer-continental shelf following the initial retreat until the early Holocene (~11.5 ka). This stabilization is not reproduced in the high mantle viscosity experiments.

A potential factor in the WAIS grounding-line stabilization that is not considered in the model simulations discussed here is sediment aggradation. In fact, grounding zone wedges in the Glomar Challenger Basin and Whales Deep Basin of the middle continental shelf show over 100 m of sediment aggradation (Bart and Owalana, 2012; Bart et al., 2017). The model simulation in which no Earth deformation scheme is used highlights the importance of isostatic uplift in West Antarctica in stabilizing the ice sheet grounding line as it retreats, but sediment aggradation could have been an equally important contributor to the stabilization of WAIS by acting as a negative feedback on grounding-line retreat (Alley et al., 2007). Future work should focus on these feedbacks between a retreating ice sheet with sediment depositional changes with coupling between ice sheet and sediment flux models.

The ERS grounding-line stabilization is difficult to reconcile with the WAIS retreat-readvance scenario of Kingslake et al. (2018) based on the presence of finite radiocarbon ages measured in the organic carbon from subglacial sediments underneath WAIS ice streams. In this scenario, the grounding line retreated beyond the modern-day position along Siple Coast in the early Holocene and readvanced to its current position due to isostatic rebound. In model simulations also using PISM, they simulate the furthest retreat in the Ross sector at 9.7 ka. Considering the radiocarbon ages from the outer continental shelf, this would indicate rapid and extensive grounding-line retreat occurring between 11.5 and 9.7 ka. With mantle viscosity of 1e21 Pa s, the maximum grounding-line retreat occurs ~6ka, but the grounding-line does not readvance to the modern Siple Coast position.

As previously mentioned, the main challenge in addressing the role of mantle viscosity is its uniform application in ice sheet models. Spatial heterogeneity of this term, which would allow for parts of the ice sheet to be more sensitive to climate forcing than others, may cause a more reasonable retreat in ice sheet models, in which the retreat occurs at a later date, but the grounding-line still achieves an accurate modern-day position following the readvance. Uncertainty in deglacial ice sheet retreat related to the lateral variations in Earth structure can be better quantified through coupling of three-dimensional (3D) spatially-variable viscoelastic Earth models with dynamic ice sheet models, though this coupling is computationally expensive. In coupled continental-scale simulations of the last deglaciation, Gomez et al. (2018) demonstrate that the use of a 3D Earth model delays ice sheet retreat relative to a 1D Earth model; the largest differences in ice thickness are observed in the Ross Embayment in the early Holocene, highlighting the significance of glacial isostatic adjustment in the deglacial ice sheet retreat history of this region.

Other controls on Siple Coast grounding-line position in the mid-to-late Holocene are ocean and precipitation forcing. Application of the WDC accumulation forcing, which has higher precipitation through the Holocene than using a constant precipitation-temperature scaling relationship, produces a thicker WAIS that is more resistant to late Holocene grounding-line retreat. Cooler ocean forcing (i.e. lower sub-shelf melt rate anomalies) also yields less extensive grounding-line retreat, and in combination with the WDC accumulation forcing, the most accurate grounding-line position is produced for the southern Siple Coast. The effect of these external forcings on modulating or driving the WAIS retreat-readvance scenario proposed in Kingslake et al. (2018) requires consideration and further exploration. The influence of the interaction of these forcings on grounding-line retreat behavior also has implications for future WAIS grounding-line changes as basal melting has been eroding the ice shelves fringing the Amundsen sector of WAIS (Pritchard et al., 2012; Favier, 2014; Seroussi et al., 2017), and Antarctic precipitation is predicted to increase (Palerme et al., 2017).

5. Conclusions

The response of ice sheet models to climate forcing has previously been shown to be highly sensitive to specific model parameters, parameterizations of physical processes, and representation of the bed (Matsuoka et al., 2015; Bart et al., 2016; Kingslake et al., 2018; Colleoni et al., 2018; Edwards et al., 2019; Seroussi et al., 2019). Here, we explore the effect of physical model parameters that control basal properties, the solid Earth, and ice flow and rheology on the ice sheet response to deglacial climate forcing in the Ross Embayment. The main conclusions are as follows:

Of the parameters explored, Φ_{min}, mantle viscosity, and E_{SSA} show the greatest influence on the broader-scale ice sheet sensitivity to climate forcing. Increasing Φ_{min} leads to increased LGM ice thickness and reduced sensitivity to deglacial climate forcing. Increasing E_{SSA}, which enhances ice shelf and ice stream velocity and basal sliding, yields higher sensitivity to climate forcing. Increasing mantle viscosity causes the ice sheet to respond rapidly to deglacial climate forcing, and with mantle viscosity >1e20 Pa s, the retreat-readvance scenario of WAIS proposed by Kingslake et al. (2018) is reproduced. In comparison to the climate forcing model ensemble, the parameter model ensemble shows larger deviation in the deglacial ice sheet evolution.

The WRS is a key area of uncertainty from both a climate forcing and model parameter selection perspective. Application of cooler climate forcing delays WRS grounding-line retreat and ice thinning in North and South Victoria Land, producing an ice sheet evolution that is more consistent with surface-exposure and marine radiocarbon records. Reducing E_{SSA}, which allows for the temporary ice shelf that fringes the EAIS outlet glaciers in the early Holocene to last for a longer duration, also delays retreat and improves consistency with surface-exposure records of individual glaciers.

The Siple Coast grounding-line evolution and extent is sensitive to mantle viscosity and Φ_{min}. A cooler ocean forcing paired with higher precipitation over WAIS during the Holocene improves the accuracy of the modern grounding-line configuration. The interaction between these model parameters and external forcings requires more exploration in order to understand grounding-line evolution in this region.

A key challenge in paleo-ice sheet modeling is the selection of model parameters and climate forcings that are representative of the given region. However, no perfect combination of model parameters or climate forcing exists, as local properties of the bed, solid Earth evolution, ice rheology and climate evolution can have large impacts on regional ice sheet evolution. These effects require consideration in model-proxy comparisons. Additional observational constraints on the rates and bed conditions of recent ice sheet grounding-line retreat are required to further improve ice sheet model parameterizations to more accurately project future responses to atmospheric and oceanic warming.

Author contributions

D.P.L. and N.R.G. devised the regional ice sheet model experiments. D.P.L. performed and analyzed the model experiments. R.S.J. provided the cosmogenic nuclide surface-exposure data. All authors contributed to the development of ideas and writing of the manuscript.

Declaration of competing interest

All authors declare that they have no competing interests.

Acknowledgements

We gratefully acknowledge A. Aschwanden and C. Khroulev for their constructive advice regarding the PISM, and the teams behind the TraCE-21ka and LOVECLIM DG_{ns} experiments for producing and sharing model output, publicly available via the NCAR Climate Data Gateway and the Asia-Pacific Data Research Center, respectively. We thank the Antarctic ice core and marine proxy communities for the use of their data. We also thank P. Bart for insightful comments that have greatly improved the manuscript. Funding for this project was provided by the Royal Society Te Aparangi Marsden Fund through Victoria University of Wellington (15-VUW-131); the New Zealand Ministry of Business, Innovation, and Employment Grant through GNS Science (540GCT32); and the New Zealand Antarctic Research Institute (NZARI2014-11). The development of PISM was supported by NASA grant NNX17AG65G and NSF grants PLR-1603799 and PLR-1644277. D.P.L. acknowledges support from the Antarctica New Zealand Doctoral Scholarship program. N.R.G. acknowledges support from the Royal Society Te Aparangi under contract VUW1501. R.S.J. was supported by a Junior Research Fellowship COFUNDed between Durham University and the European Union under grant agreement number 609412. R.M. acknowledges support from the Royal Society Te Aparangi Rutherford Discovery Fellowship (RDF-13-VUW-003). N.A.N.B. acknowledges support from the Royal Society Te Aparangi Rutherford Discovery Fellowship (RDF-VUW-1103).

References

Ackert Jr., R.P., Putnam, A.E., Mukhopadhyay, S., Pollard, D., DeConto, R.M., Kurz, M.D., Borns Jr., H.W., 2013. Controls on interior West Antarctic Ice Sheet Elevations: inferences from geologic constraints and ice sheet modeling. Quat. Sci. Rev. 65, 26–38.

Alley, R.B., Blankenship, D.D., Bentley, C.R., Rooney, S.T., 1986. Deformation of till beneath ice stream B, West Antarctica. Nature 322 (6074), 57.

Alley, R.B., Anandakrishnan, S., Dupont, T.K., Parizek, B.R., Pollard, D., 2007. Effect of sedimentation on ice-sheet grounding-line stability. Science 315 (5820), 1838–1841.

Anderson, J.B., Conway, H., Bart, P.J., Witus, A.E., Greenwood, S.L., McKay, R.M., et al., 2014. Ross Sea paleo-ice sheet drainage and deglacial history during and since the LGM. Quat. Sci. Rev. 100, 31–54.

Anderson, J.B., Simkins, L.M., Bart, P.J., De Santis, L., Halberstadt, A.R.W., Olivo, E., Greenwood, S.L., 2019. Seismic and geomorphic records of Antarctic Ice Sheet evolution in the Ross Sea and controlling factors in its behaviour. Geological Society, London, Special Publications 475 (1), 223–240.

Anderson, J.T., Wilson, G.S., Fink, D., Lilly, K., Levy, R.H., Townsend, D., 2017. Reconciling marine and terrestrial evidence for post LGM ice sheet retreat in southern McMurdo Sound, Antarctica. Quat. Sci. Rev. 157, 1–13.

Argus, D.F., Peltier, W.R., Drummond, R., Moore, A.W., 2014. The Antarctica component of postglacial rebound model ICE-6G_C (VM5a) based on GPS positioning, exposure age dating of ice thicknesses, and relative sea level histories. Geophys. J. Int. 198 (1), 537–563.

Aschwanden, A., Aðalgeirsdóttir, G., Khroulev, C., 2013. Hindcasting to measure ice sheet model sensitivity to initial states. Cryosphere 7 (4).

Baroni, C., Noti, V., Ciccacci, S., Righini, G., Salvatore, M.C., 2005. Fluvial origin of the valley system in northern Victoria Land (Antarctica) from quantitative geomorphic analysis. Geol. Soc. Am. Bull. 117 (1–2), 212–228.

Bart, P.J., Owolana, B., 2012. On the duration of West Antarctic ice sheet grounding events in Ross Sea during the quaternary. Quat. Sci. Rev. 47, 101–115.

Bart, P.J., Mullally, D., Golledge, N.R., 2016. The influence of continental shelf bathymetry on Antarctic Ice Sheet response to climate forcing. Glob. Planet. Chang. 142, 87–95.

Bart, P.J., Krogmeier, B.J., Bart, M.P., Tulaczyk, S., 2017. The paradox of a long grounding during West Antarctic ice sheet retreat in Ross Sea. Sci. Rep. 7 (1), 1262.

Bart, P.J., DeCesare, M., Rosenheim, B.E., Majewski, W., McGlannan, A., 2018. A centuries-long delay between a paleo-ice-shelf collapse and grounding-line retreat in the Whales Deep Basin, eastern Ross Sea, Antarctica. Sci. Rep. 8 (1), 12392.

Behrendt, J.C., Cooper, A., 1991. Evidence of rapid Cenozoic uplift of the shoulder escarpment of the Cenozoic West Antarctic rift system and a speculation on possible climate forcing. Geology 19 (4), 315–319.

Bentley, M.J., Fogwill, C.J., Le Brocq, A.M., Hubbard, A.L., Sugden, D.E., Dunai, T.J., Freeman, S.P., 2010. Deglacial history of The west antarctic ice sheet in the Weddell Sea embayment: constraints on past ice volume change. Geology 38 (5), 411–414.

Borchers, B., Marrero, S., Balco, G., Caffee, M., Goehring, B., Lifton, N., et al., 2016. Geological calibration of spallation production rates in the CRONUS-Earth project. Quat. Geochronol. 31, 188–198.

Bueler, E., Brown, J., 2009. Shallow shelf approximation as a "sliding law" in a thermomechanically coupled ice sheet model. J. Geophys. Res.: Earth Surface 114 (F3).

Bueler, E.D., Lingle, C.S., Brown, J., 2007. Fast computation of a viscoelastic deformable Earth model for ice-sheet simulations. Ann. Glaciol. 46, 97–105.

Colleoni, F., De Santis, L., Montoli, E., Olivo, E., Sorlien, C.C., Bart, P.J., et al., 2018. Past continental shelf evolution increased Antarctic ice sheet sensitivity to climatic conditions. Sci. Rep. 8 (1), 11323.

Conway, H., Hall, B.L., Denton, G.H., Gades, A.M., Waddington, E.D., 1999. Past and future grounding-line retreat of The west antarctic ice sheet. Science 286 (5438), 280–283.

Cuffey, K.M., Clow, G.D., Steig, E.J., Buizert, C., Fudge, T.J., Koutnik, M., et al., 2016. Deglacial temperature history of West Antarctica. Proc. Natl. Acad. Sci. 113 (50), 14249–14254.

de Boer, B., Dolan, A.M., Bernales, J., Gasson, E., Golledge, N.R., Sutter, J., et al., 2015. Simulating the Antarctic ice sheet in the late-Pliocene warm period: PLISMIP-ANT, an ice-sheet model intercomparison project. Cryosphere 9, 881–903.
DeConto, R.M., Pollard, D., 2016. Contribution of Antarctica to past and future sea-level rise. Nature 531 (7596), 591.
Deschamps, P., Durand, N., Bard, E., Hamelin, B., Camoin, G., Thomas, A.L., et al., 2012. Ice-sheet collapse and sea-level rise at the Bølling warming 14,600 years ago. Nature 483 (7391), 559.
Dinniman, M.S., Klinck, J.M., Hofmann, E.E., Smith Jr., W.O., 2018. Effects of projected changes in wind, atmospheric temperature, and freshwater inflow on the Ross Sea. J. Clim. 31 (4), 1619–1635.
Domack, E.W., Jacobson, E.A., Shipp, S., Anderson, J.B., 1999. Late pleistocene–holocene retreat of The west antarctic ice-sheet system in the Ross Sea: Part 2—sedimentologic and stratigraphic signature. Geol. Soc. Am. Bull. 111 (10), 1517–1536.
Edwards, T.L., Brandon, M.A., Durand, G., Edwards, N.R., Golledge, N.R., Holden, P.B., et al., 2019. Revisiting Antarctic ice loss due to marine ice-cliff instability. Nature 566 (7742), 58.
Elderfield, H., Ferretti, P., Greaves, M., Crowhurst, S., McCave, I.N., Hodell, D.A., Piotrowski, A.M., 2012. Evolution of ocean temperature and ice volume through the mid-Pleistocene climate transition. Science 337 (6095), 704–709.
Favier, L., Durand, G., Cornford, S.L., Gudmundsson, G.H., Gagliardini, O., Gillet-Chaulet, F., et al., 2014. Retreat of Pine Island Glacier controlled by marine ice-sheet instability. Nat. Clim. Chang. 4 (2), 117.
Fretwell, P., Pritchard, H.D., Vaughan, D.G., Bamber, J.L., Barrand, N.E., Bell, R., et al., 2013. Bedmap2: improved ice bed, surface and thickness datasets for Antarctica. Cryosphere 7, 375–393.
Fudge, T.J., Markle, B.R., Cuffey, K.M., Buizert, C., Taylor, K.C., Steig, E.J., et al., 2016. Variable relationship between accumulation and temperature in West Antarctica for the past 31,000 years. Geophys. Res. Lett. 43 (8), 3795–3803.
Goehring, B.M., Balco, G., Todd, C., Moening-Swanson, I., Nichols, K., 2019. Late-glacial grounding line retreat in the northern Ross Sea, Antarctica. Geology 47 (4), 291–294.
Golledge, N.R., Menviel, L., Carter, L., Fogwill, C.J., England, M.H., Cortese, G., Levy, R.H., 2014. Antarctic contribution to meltwater pulse 1A from reduced Southern Ocean overturning. Nat. Commun. 5, 5107.
Golledge, N.R., Kowalewski, D.E., Naish, T.R., Levy, R.H., Fogwill, C.J., Gasson, E.G., 2015. The multi-millennial Antarctic commitment to future sea-level rise. Nature 526 (7573), 421.
Golledge, N.R., Keller, E.D., Gomez, N., Naughten, K.A., Bernales, J., Trusel, L.D., Edwards, T.L., 2019. Global environmental consequences of twenty-first-century ice-sheet melt. Nature 566 (7742), 65.
Gomez, N., Mitrovica, J.X., Huybers, P., Clark, P.U., 2010. Sea level as a stabilizing factor for marine-ice-sheet grounding lines. Nat. Geosci. 3 (12), 850.
Gomez, N., Latychev, K., Pollard, D., 2018. A coupled ice sheet–sea level model incorporating 3D earth structure: variations in Antarctica during the last deglacial retreat. J. Clim. 31 (10), 4041–4054.
Greenwood, S.L., Simkins, L.M., Halberstadt, A.R.W., Prothro, L.O., Anderson, J.B., 2018. Holocene reconfiguration and readvance of the east antarctic ice sheet. Nat. Commun. 9.
Halberstadt, A.R.W., Simkins, L.M., Greenwood, S.L., Anderson, J.B., 2016. Past ice-sheet behaviour: retreat scenarios and changing controls in the Ross Sea, Antarctica. Cryosphere 10, 1003–1020.
Hellmer, H.H., 2004. Impact of Antarctic ice shelf basal melting on sea ice and deep ocean properties. Geophys. Res. Lett. 31 (10).
Hillenbrand, C.D., Smith, J.A., Hodell, D.A., Greaves, M., Poole, C.R., Kender, S., et al., 2017. West Antarctic Ice Sheet retreat driven by Holocene warm water incursions. Nature 547 (7661), 43.
Hulbe, C.L., Scambos, T.A., Klinger, M., Fahnestock, M.A., 2016. Flow variability and ongoing margin shifts on bindschadler and MacAyeal ice streams, west Antarctica. J. Geophys. Res.: Earth Surface 121 (2), 283–293.
Huybrechts, P., de Wolde, J., 1999. The dynamic response of the Greenland and Antarctic ice sheets to multiple-century climatic warming. J. Clim. 12 (8), 2169–2188.
Jones, R.S., Mackintosh, A.N., Norton, K.P., Golledge, N.R., Fogwill, C.J., Kubik, P.W., et al., 2015. Rapid Holocene thinning of an East Antarctic outlet glacier driven by marine ice sheet instability. Nat. Commun. 6, 8910.
Kingslake, J., Scherer, R.P., Albrecht, T., Coenen, J., Powell, R.D., Reese, R., et al., 2018. Extensive retreat and re-advance of The west antarctic ice sheet during the Holocene. Nature 558 (7710), 430.
Lee, J.I., McKay, R.M., Golledge, N.R., Yoon, H.I., Yoo, K.C., Kim, H.J., Hong, J.K., 2017. Widespread persistence of expanded East Antarctic glaciers in the southwest Ross Sea during the last deglaciation. Geology 45 (5), 403–406.
Licht, K.J., Andrews, J.T., 2002. The 14C record of Late Pleistocene ice advance and retreat in the central Ross Sea, Antarctica. Arctic Antarct. Alpine Res. 34 (3), 324–333.
Lisiecki, L.E., Raymo, M.E., 2005. A Pliocene-Pleistocene stack of 57 globally distributed benthic δ18O records. Paleoceanography 20 (1).
Liu, Z., Otto-Bliesner, B.L., He, F., Brady, E.C., Tomas, R., Clark, P.U., et al., 2009. Transient simulation of last deglaciation with a new mechanism for Bølling-Allerød warming. Science 325 (5938), 310–314.
Lowry, D.P., Golledge, N.R., Bertler, N.A.N., Jones, R.S., McKay, R., 2019a. Deglacial grounding-line retreat in the Ross Embayment, Antarctica, controlled by ocean and atmosphere forcing. Sci. Adv. 5.
Lowry, D.P., Golledge, N.R., Menviel, L., Bertler, N.A., 2019b. Deglacial evolution of regional Antarctic climate and Southern Ocean conditions in transient climate simulations. Clim. Past 15 (1), 189–215.
Martin, M.A., Winkelmann, R., Haseloff, M., Albrecht, T., Bueler, E., Khroulev, C., Levermann, A., 2011. The potsdam parallel ice sheet model (PISM-PIK)–Part 2: dynamic equilibrium simulation of the antarctic ice sheet. Cryosphere 5 (3), 727–740.
Matsuoka, K., Hindmarsh, R.C., Moholdt, G., Bentley, M.J., Pritchard, H.D., Brown, J., et al., 2015. Antarctic ice rises and rumples: their properties and significance for ice-sheet dynamics and evolution. Earth Sci. Rev. 150, 724–745.
McKay, R., Golledge, N.R., Maas, S., Naish, T., Levy, R., Dunbar, G., Kuhn, G., 2016. Antarctic marine ice-sheet retreat in the Ross Sea during the early Holocene. Geology 44 (1), 7–10.
Menviel, L., Timmermann, A., Timm, O.E., Mouchet, A., 2011. Deconstructing the Last Glacial termination: the role of millennial and orbital-scale forcings. Quat. Sci. Rev. 30 (9–10), 1155–1172.
Palerme, C., Genthon, C., Claud, C., Kay, J.E., Wood, N.B., L'Ecuyer, T., 2017. Evaluation of current and projected Antarctic precipitation in CMIP5 models. Clim. Dyn. 48 (1–2), 225–239.
Pattyn, F., Favier, L., Sun, S., Durand, G., 2017. Progress in numerical modeling of Antarctic ice-sheet dynamics. Current climate change reports 3 (3), 174–184.
Parrenin, F., Barnola, J.M., Beer, J., Blunier, T., Castellano, E., Chappellaz, J., et al., 2007. The EDC3 chronology for the EPICA Dome C ice core. Clim. Past 3, 485–497.
Peltier, W.R., 2004. Global glacial isostasy and the surface of the ice-age Earth: the ICE-5G (VM2) model and GRACE. Annu. Rev. Earth Planet Sci. 32, 111–149.
The PISM authors, 2017. PISM, a Parallel Ice Sheet Model: User's Manual (2017) based on development revision e9d2d1f8 (7 March 2017). http://www.pismdocs.org/wiki/lib/exe/fetch.php?media=pism_manual.pdf.
Pollard, D., DeConto, R.M., 2009. Modelling West Antarctic ice sheet growth and collapse through the past five million years. Nature 458 (7236), 329.
Pollard, D., DeConto, R.M., Alley, R.B., 2015. Potential Antarctic Ice Sheet retreat driven by hydrofracturing and ice cliff failure. Earth Planet. Sci. Lett. 412, 112–121.
Pritchard, H., Ligtenberg, S.R.M., Fricker, H.A., Vaughan, D.G., Van den Broeke, M.R., Padman, L., 2012. Antarctic ice-sheet loss driven by basal melting of ice shelves. Nature 484 (7395), 502.
Rignot, E., Bamber, J.L., Van Den Broeke, M.R., Davis, C., Li, Y., Van De Berg, W.J., Van Meijgaard, E., 2008. Recent Antarctic ice mass loss from radar interferometry and regional climate modelling. Nat. Geosci. 1 (2), 106.
Seroussi, H., Nakayama, Y., Larour, E., Menemenlis, D., Morlighem, M., Rignot, E., Khazendar, A., 2017. Continued retreat of Thwaites Glacier, West Antarctica, controlled by bed topography and ocean circulation. Geophys. Res. Lett. 44 (12), 6191–6199.
Seroussi, H., Nowicki, S., Simon, E., Abe-Ouchi, A., Albrecht, T., Brondex, J., Cornford, S., Dumas, C., Gillet-Chaulet, F., Goelzer, H., et al., 2019. initMIP-Antarctica: an ice sheet model initialization experiment of ISMIP6. Cryosphere 13 (5), 1441–1471.
Shipp, S., Anderson, J., Domack, E., 1999. Late pleistocene–holocene retreat of The west antarctic ice-sheet system in the Ross Sea: part 1—geophysical results. Geol. Soc. Am. Bull. 111 (10), 1486–1516.
Simkins, L.M., Anderson, J.B., Greenwood, S.L., 2016. Glacial landform assemblage reveals complex retreat of grounded ice in the Ross Sea, Antarctica. Geological Society, London, Memoirs 46 (1), 353–356.
Spector, P., Stone, J., Cowdery, S.G., Hall, B., Conway, H., Bromley, G., 2017. Rapid early-holocene deglaciation in the Ross Sea, Antarctica. Geophys. Res. Lett. 44 (15), 7817–7825.
Stone, J.O., Balco, G.A., Sugden, D.E., Caffee, M.W., Sass, L.C., Cowdery, S.G., Siddoway, C., 2003. Holocene deglaciation of Marie Byrd land. west Antarctica. Science 299 (5603), 99–102.
Tinto, K.J., Padman, L., Siddoway, C.S., Springer, S.R., Fricker, H.A., Das, I., et al., 2019. Ross Ice Shelf response to climate driven by the tectonic imprint on seafloor bathymetry. Nat. Geosci. 1.
Todd, C., Stone, J., Conway, H., Hall, B., Bromley, G., 2010. Late quaternary evolution of Reedy Glacier, Antarctica. Quat. Sci. Rev. 29 (11–12), 1328–1341.
Tulaczyk, S., Kamb, W.B., Engelhardt, H.F., 2000. Basal mechanics of ice stream B, West Antarctica: 1. Till mechanics. J. Geophys. Res.: Solid Earth 105 (B1), 463–481.
Whitehouse, P.L., Gomez, N., King, M.A., Wiens, D.A., 2019. Solid earth change and the evolution of the antarctic ice sheet. Nat. Commun. 10 (1), 503.
Winkelmann, R., Martin, M.A., Haseloff, M., Albrecht, T., Bueler, E., Khroulev, C., Levermann, A., 2011. The Potsdam parallel ice sheet model (PISM-PIK)–Part 1: model description. Cryosphere 5 (3), 715–726.
Yokoyama, Y., Anderson, J.B., Yamane, M., Simkins, L.M., Miyairi, Y., Yamazaki, T., et al., 2016. Widespread collapse of the Ross ice shelf during the late Holocene. Proc. Natl. Acad. Sci. 113 (9), 2354–2359.